Cell

Regulation of Transcription through Acetylation of H3K122 on the Lateral Surface of the Histone Octamer

Philipp Tropberger,[1,2] Sebastian Pott,[3,10] Claudia Keller,[4,5] Kinga Kamieniarz-Gdula,[1,11] Matthieu Caron,[6,7,8] Florian Richter,[1] Guohong Li,[9] Gerhard Mittler,[1] Edison T. Liu,[3,12] Marc Bühler,[4,5] Raphael Margueron,[6,7,8] and Robert Schneider[1,2,*]

[1]Max Planck Institute of Immunobiology and Epigenetics, 79108 Freiburg, Germany
[2]Institut de Génétique et de Biologie Moléculaire et Cellulaire, CNRS UMR 7104, INSERM U 964, Université de Strasbourg, 67404 Illkirch, France
[3]Cancer Biology and Pharmacology, Genome Institute of Singapore, Singapore 138672, Republic of Singapore
[4]Friedrich Miescher Institute for Biomedical Research, Maulbeerstrasse 66, 4058 Basel, Switzerland
[5]University of Basel, Petersplatz 10, 4003 Basel, Switzerland
[6]Institut Curie, 26 rue d'Ulm, 75005 Paris, France
[7]UMR 3215 CNRS, 26 rue d'Ulm, 75005 Paris, France
[8]U934 INSERM, 26 rue d'Ulm, 75005 Paris, France
[9]National Laboratory of Biomacromolecules, Institute of Biophysics, Chinese Academy of Sciences, Beijing 100101, People's Republic of China
[10]Present address: Department of Biology, University of North Carolina at Chapel Hill, NC 27599-3280, USA
[11]Present address: Sir William Dunn School of Pathology, University of Oxford, South Parks Road, Oxford OX1 3RE, UK
[12]Present address: The Jackson Laboratory, 600 Main Street, Bar Harbor, ME 04609, USA
*Correspondence: schneidr@igbmc.fr
http://dx.doi.org/10.1016/j.cell.2013.01.032

SUMMARY

Histone modifications are key regulators of chromatin function. However, little is known to what extent histone modifications can directly impact on chromatin. Here, we address how a modification within the globular domain of histones regulates chromatin function. We demonstrate that H3K122ac can be sufficient to stimulate transcription and that mutation of H3K122 impairs transcriptional activation, which we attribute to a direct effect of H3K122ac on histone-DNA binding. In line with this, we find that H3K122ac defines genome-wide genetic elements and chromatin features associated with active transcription. Furthermore, H3K122ac is catalyzed by the coactivators p300/CBP and can be induced by nuclear hormone receptor signaling. Collectively, this suggests that transcriptional regulators elicit their effects not only via signaling to histone tails but also via direct structural perturbation of nucleosomes by directing acetylation to their lateral surface.

INTRODUCTION

Each of the four core histones—H3, H2A, H2B, and H4—can be divided into two structurally and functionally distinct domains: a globular domain that forms the scaffold around which DNA is wrapped and flexible unstructured tails protruding from the nucleosomal core. These histone tails are largely dispensable for nucleosome formation per se (Ausio et al., 1989) but can serve as platforms for a variety of posttranslational modifications (PTMs) (Kouzarides, 2007). These PTMs have the potential to govern chromatin function, according to the "histone code" hypothesis (Strahl and Allis, 2000; Turner, 2000), mainly by recruiting or repelling specific binding or "effector" proteins. Whereas the function of histone tails as highly modified "signaling platforms" is generally accepted, the globular domains have long been seen as simple structural scaffolds. However, PTMs have also been detected within the globular domains (Cocklin and Wang, 2003; Freitas et al., 2004; Garcia, 2009). Many of these PTMs map to residues located on the lateral surface of the histone octamer and are in direct or water-mediated contact with the nucleosomal DNA (Freitas et al., 2004). Based on their critical location, Cosgrove et al. (2004) proposed a model of "regulated nucleosome mobility" according to which modifications on the lateral surface could, in contrast to most PTMs in the histone tails, directly affect nucleosome and chromatin dynamics without depending on recognition by effector proteins. Within the globular domain of H3, four lysine residues map to the lateral surface: K56, K64, K115, and K122. All four lysines can potentially be acetylated (Tropberger and Schneider, 2010). H3K122 is located on the dyad axis of the nucleosome, which is the part of the lateral surface where histone-DNA binding reaches its maximum strength (Hall et al., 2009). Replacing H3K122 with an acetyllysine-mimicking glutamine residue results in the loss of a water-mediated salt bridge between H3K122 and the DNA in the dyad axis (Iwasaki et al., 2011),

suggesting that potential acetylation of H3K122 could act to destabilize histone-DNA binding. In line with this, it was found that in vitro acetylation in the dyad axis can enhance the rate of nucleosome disassembly upon mechanical stress (Simon et al., 2011). In vivo first evidence for acetylation of H3K122 has been detected on bovine and human histones by mass spectrometry (Tan et al., 2011; Zhang et al., 2003). However, the role of H3K122ac in chromatin has not yet been addressed. We therefore set out to functionally characterize acetylation of H3K122 in vitro and in vivo.

We show that in vivo H3K122ac is enriched at genetic elements associated with transcriptional activation genome wide. In line with a role for promoting transcription, acetylation of H3K122 is dependent on the transcriptional coactivator p300/CREB-binding protein (CBP) and is dynamically regulated by estrogen receptor signaling. Despite the coexistence of H3K122ac with other H3 tail acetylations in the same nucleosome, we found that H3K122ac—in contrast to a single H3 tail acetylation—can be sufficient to stimulate transcription and histone eviction. Furthermore, we demonstrate that mutation of K122 can result in impaired gene induction in vivo.

RESULTS

H3K122ac Is Ubiquitously Present in Higher Eukaryotes

To address the functional importance of modifications on the lateral surface of the histone octamer, we focused on acetylation of H3K122, located close to the dyad symmetry axis (Figure 1A), which is a region of major importance for nucleosome stability (Hall et al., 2009). By mass spectrometric analysis, we confirmed acetylation of H3K122 in cells of human and murine origin (Figure S1A available online).

To gain insight into the function of H3K122ac, we first performed an exhaustive characterization of an antibody raised against acetylated H3K122. This antibody specifically recognizes histone H3 in nuclear extract from human MCF-7 breast cancer cells (Figure 1B). This signal can be increased by treatment of cells with a histone deacetylase inhibitor, demonstrating that, indeed, acetylation is detected (Figure 1C). The antibody is highly specific for synthetic peptides with H3K122ac over peptides with previously described acetyl marks in histone tails and globular domains, both in dot-blot and in competition assays (Figures S1B and S1C). To further exclude potential cross-reactivity with histone tail modifications, we digested native nucleosomes with a limited amount of trypsin to remove the tails. Removal of the H3 tail did not reduce the signal detected by the H3K122ac antibody (Figure 1D). Taken together, these data provide compelling evidence that the antibody used recognizes H3K122ac with high specificity.

By immunoblot, we detected H3K122ac in histones from different higher eukaryotes, including human, mouse, and fly, as well as in different mouse tissues (Figures S1D and S1E), suggesting a rather ubiquitous presence of H3K122ac. We estimate that, on average, 1 out of 250 nucleosomes is acetylated at H3K122ac in untreated cells (Figure S1F). To gain insight in the nuclear distribution of H3K122ac, we performed immunofluorescence microscopy in mouse embryonic fibroblasts. H3K122ac appeared uniformly distributed within the nucleus but excluded from DAPI-rich pericentromeric heterochromatic regions (Figure 1E). This localization pattern is euchromatic and suggests a localization of H3K122ac to ''active'' chromatin.

Nucleosomes with H3K122ac Are Enriched for Active Histone Marks at the Transcription Start Site of Transcribed Genes

To study the distribution of H3K122ac within chromatin, we first asked whether H3K122ac co-occurs with specific histone marks on the same nucleosome. We purified mononucleosomes from MCF-7 cells (Figures S2A–S2C), immunoprecipitated them with the H3K122ac antibody, and probed with antibodies recognizing other histone modifications (Figure 2A). H3K122ac-containing nucleosomes were globally enriched for acetyl marks on both histone H3 and H4 (Figure 2A, right). Additionally, H3K122ac co-occurred with a number of methyl marks, such as H3K4me1, which is enriched mainly at distal enhancers, and with H3K4me3, which predominantly locates to active promoters (Heintzman et al., 2007; Zhou et al., 2010). In contrast, PTMs associated with facultative heterochromatin (H3K27me3), constitutive heterochromatin (H3K9me3) (Bannister and Kouzarides, 2011), or the gene body of actively transcribed genes (H3K36me3) (Krogan et al., 2003) were not enriched in H3K122ac nucleosomes (Figure 2A, left).

In addition to histone marks, the distribution of histone variants differs between distinct chromatin states. The histone variant H2A.Z is generally present at promoters and enhancers (Barski et al., 2007), and acetylated H2A.Z (H2A.Zac) is strongly enriched at active promoters (Valdés-Mora et al., 2012). We found that H2A.Z and H2A.Zac co-occur with H3K122ac (Figure 2B). The histone variant H3.3 is enriched in specific genomic regions, including enhancers and transcribed genes (Goldberg et al., 2010). Immunoblot for H3K122ac on ectopically expressed HA/FLAG-H3.1 and -H3.3 revealed significant enrichment of H3K122ac on the ''active'' variant H3.3 compared to H3.1 (Figures 2C and S2D). Altogether, these results suggest a global association of H3K122ac with marks and features of euchromatin and a preferred localization to active gene promoters and potentially to enhancers.

To determine the genome-wide distribution of H3K122ac, we used chromatin immunoprecipitation sequencing (ChIP-seq) coupled with next-generation sequencing. Sites of H3K122ac enrichment showed overall reduced nucleosome density (Figure S2E), which is in line with enrichment of H3K122ac in ''open'' euchromatin. We found H3K122ac enriched in distinct peaks or small regions of multiple peaks (Figure 2D), of which 43% percent map to gene promoters (Figure 2E). The distribution of H3K122ac at individual promoters (Figure 2F) suggests that H3K122ac is enriched close to the transcription start site (TSS). To further analyze this, we aligned all coding genes by their TSS (for TSS of noncoding transcripts, see Figure S2F) and plotted the average read distribution for H3K122ac. H3K122ac is globally enriched in two main peaks flanking the TSS (Figure 2G) with a relatively high level of enrichment upstream of the TSS. This H3K122ac pattern is overall more similar to H2A.Zac and H3K27ac distribution rather than to H3K9ac and H3K4me3 and does not extend far into the gene body, which is in agreement with the low levels of H3K36me3 on H3K122ac

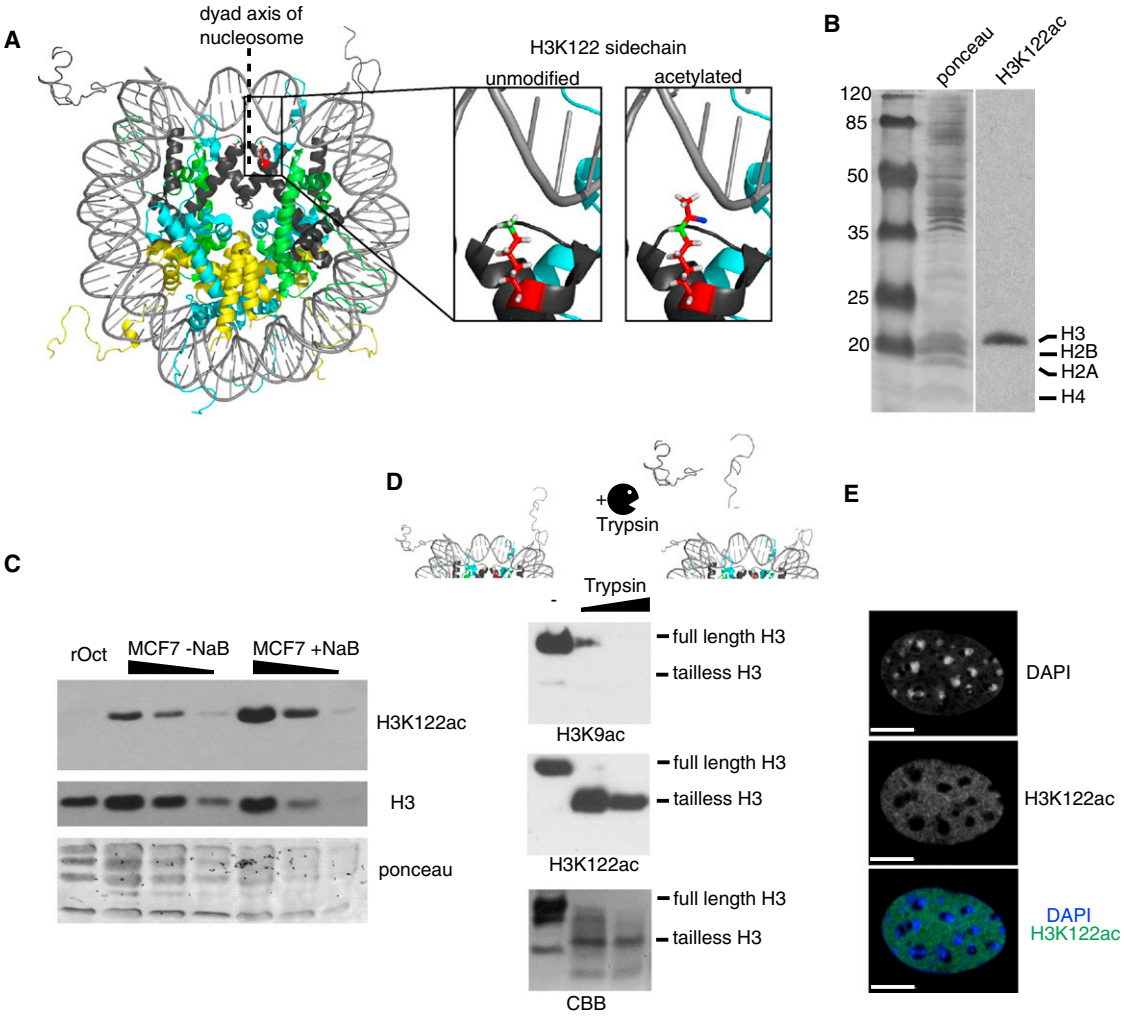

Figure 1. Antibody Specific for H3K122ac, Located at the Dyad Axis of the Nucleosome

(A) Model of a nucleosome based on Protein Data Bank (PDB) code 1KX5. The dotted line marks the dyad axis of the nucleosome (left). K122 on histone H3 (black) in proximity to the dyad axis is shown in both unmodified (middle) and acetylated states (right).

(B) The antibody raised against H3K122ac detects a single band (right) in immunoblots of whole-nuclei extract from MCF-7 cells (Ponceau staining and marker, left).

(C) H3K122ac immunoblot of recombinant histone octamers (rOct) and native, acid-extracted histones from MCF-7 cells treated ±10 mM NaB overnight. Ponceau staining and immunoblot for H3 are shown as loading controls.

(D) The H3K122ac antibody detects globular, tailless H3. Nucleosomes from MCF-7 cells were incubated with no (−) or increasing amounts of trypsin to cleave the histone tails and immunoblotted for H3K9ac (top) and H3K122ac (middle). The position of full-length and tailless H3 is indicated in the Coomassie brilliant blue staining (CBB, bottom).

(E) Immunofluorescence analysis of H3K122ac in mouse embryonic fibroblasts. DNA was stained with DAPI (top); the bright foci mark pericentromeric heterochromatin. The signal for H3K122ac (middle) is excluded from the DAPI dense foci as shown in the merge (bottom). Scale bar is 10 μm.

See Figure S1 for mass spectrometry and additional information.

nucleosomes (Figure 2A). The levels of H3K122ac at the TSS correlate highly with the levels of gene expression (Figures 2G and S2F). Quantitative comparison of H3K122ac with other chromatin modifications revealed a high correlation for H3K122ac with H2A.Zac (Figure 2H) and H3K27ac, whereas, for example, H3K4me3 enrichment showed only modest correlation with H3K122ac. Because H2A.Zac is a strong indicator of transcriptional output (Valdés-Mora et al., 2012), this points again toward a role of H3K122ac in transcription.

H3K122ac Directly Stimulates Transcription In Vitro

Having established H3K122ac as a histone modification that is associated with chromatin marks and genetic elements of active transcription, we next aimed to directly test whether H3K122ac contributes functionally to transcription. To this end, we developed an in vitro transcription (IVT) assay with recombinant chromatin containing a single acetylation on H3. We produced recombinant H3 acetylated at either H3K122 or H3K18 (in the middle of the H3 tail as a control) in *Escherichia coli* using

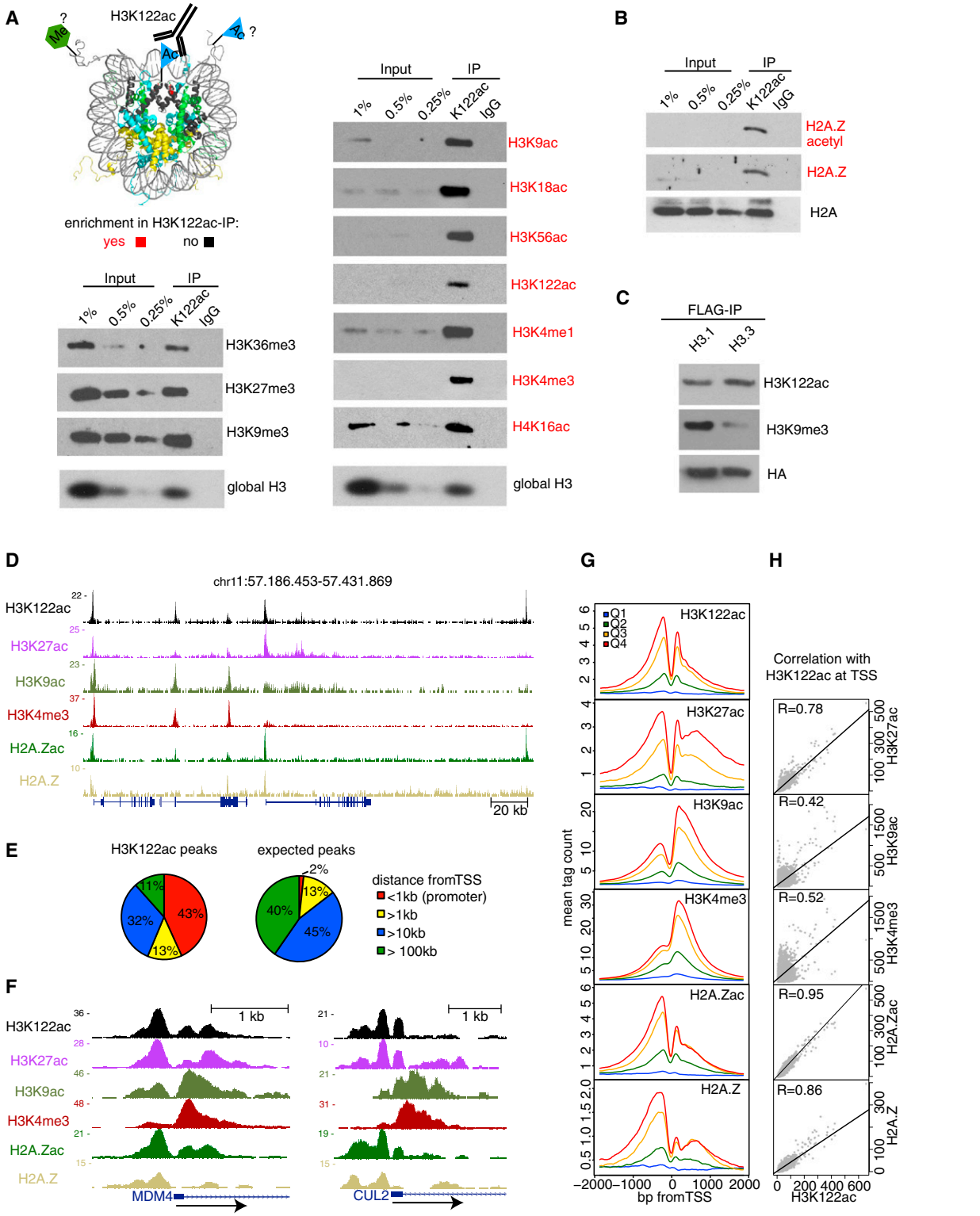

Figure 2. H3K122ac Nucleosomes Are Enriched in Histone Modifications and Variants Associated with Open Chromatin at TSS

(A) Enrichment of specific histone modifications within H3K122ac nucleosomes. Pure mononucleosomes from MCF-7 cells were immunoprecipitated with the H3K122ac or IgG control antibody and immunoblotted with the indicated antibodies. Histone modifications that were enriched by H3K122ac immunoprecipitation relative to input are highlighted in red.

(B) H2A.Z is enriched in H3K122ac mononucleosomes. The amount of the histone variant H2A.Z and acetylated H2A.Z compared to H2A as in (A).

(legend continued on next page)

site-specific genetically directed incorporation of acetyllysine (Neumann et al., 2009). Because IVT assays with chromatin require a step of acetylation for efficient transcription (Figure 3A), we included an H3K122R mutant as a nonacetylatable H3K122 control. We refolded and purified recombinant histone octamers with one of four different H3s (wild-type [WT] H3, H3K122R, H3K122ac, or H3K18ac) (Figures 3B and S3A) and assembled chromatin with the histone chaperone NAP1 and the ACF (ATP-dependent chromatin assembly factor) remodeling complex (Figure S3B) on the pG5-MLP plasmid. We then compared successfully assembled (Figure S3C) and purified chromatin in IVT assays. Interestingly, we found that (under conditions permissive for efficient transcription of chromatin) H3K122ac is sufficient to cause an increase in transcription compared to chromatin with H3wt, H3K122R, and, importantly, H3K18ac histones (Figure 3C). On average, acetylation of H3K122 stimulates transcription by ~1.7-fold ($p = 0.02$) (Figure 3D). Because only H3K122ac, but not the H3K122R mutation, enhanced transcription, this experiment demonstrates that stimulation of transcription by H3K122ac is not a general phenomenon due to alteration of H3K122.

H3K122ac did not change chromatin compaction in general (analytical ultracentrifugation, data not shown) and also did not change chromatin decompaction upon acetylation in a detectable manner (Figures S3D and S3E), raising the question of how H3K122ac mechanistically stimulates transcription. To address which step of the transcription reaction is affected by H3K122ac, we performed in vitro ChIP on pG5-MLP chromatin assembled with H3K122R and H3K122ac octamers and compared the recruitment of preinitiation complex (PIC) members. Our in vitro ChIP revealed increased binding of GAL4-VP16 as well as recruitment of RNA polymerase II (Pol II) and the mediator subunit Med23 to pG5-MLP chromatin with H3K122ac relative to H3K122R chromatin (Figure 3E). Because it has been demonstrated that GAL4 binding to nucleosomal DNA competes with histones (Owen-Hughes and Workman, 1996; Workman and Kingston, 1992), we investigated whether the observed increase in GAL4-VP16 binding and Pol II/Med23 recruitment to H3K122ac chromatin (Figure 3E) is due to stimulation of histone displacement by H3K122ac. To test this, we assembled chromatin with H3K122R or H3K122ac octamers on a short linear DNA template containing the five GAL4 binding sites and the promoter of the pG5-MLP plasmid (Figure S3F) and performed a histone eviction assay (Figures 3F and S3G). We detected more H3 in the evicted fraction from H3K122ac chromatin than from H3K122R chromatin (Figure 3G), demonstrating that H3K122ac can indeed stimulate histone eviction. The same was observed when chromatin was assembled with a mixture of H3K122R and H3K122ac octamers (Figure S3H). Taken together, these experiments show that H3K122ac stimulates transcription, which we attribute to a stimulation of histone eviction and increased binding of transcriptional activator as well as recruitment of mediator (subunit Med 23) and Pol II.

H3K122ac Is Dynamically Regulated at Estrogen Receptor Targets

Having demonstrated that H3K122ac correlates with and functionally contributes to transcription, we next investigated how the level of H3K122ac is regulated upon transcriptional activation in vivo. To test this, we analyzed the dynamics of H3K122ac levels at the estrogen-responsive *TFF1(pS2)* gene promoter upon ERα-mediated gene activation in MCF-7 cells (Figure S4A), a well-studied model system for gene regulation by nuclear hormone receptors. The *TFF1(pS2)* promoter contains an estrogen-responsive element (ERE) that is bound by ERα upon estrogen stimulation (Figure S4B) and is partially occupied by a nucleosome (NucE), followed by another nucleosome that partially occupies the TATA box (NucT) (Sewack and Hansen, 1997) (Figure 4A). We found that, upon addition of estrogen, H3K122ac levels increase rapidly at the NucE and NucT position (maximum within 10 min), closely followed by Pol II loading (maximum after 20 min). In contrast to this, H3K4me3 levels increase only after 40 min and predominantly increase at the NucT position closer to the TSS. Overall, this time course shows that H3K122ac is rapidly induced upon estrogen stimulation. Furthermore, together with the global enrichment of H3K122ac at ERα binding sites (Figure S4C), this suggests that H3K122 can be acetylated by an enzymatic activity recruited by ERα.

ERα has been reported to recruit coactivators with histone acetyltransferase (HAT) activity such as p300 (and its paralog CBP), pCAF, and TIP60 (Perissi and Rosenfeld, 2005). An ERα-IP from MCF-7 nuclear extract did indeed enrich for an activity acetylating H3K122 in an in vitro HAT reaction (Figure 4B), and this activity was higher upon estrogen treatment (Figure 4B, compare lanes 7 and 9). The addition of C646, a HAT inhibitor specific for p300/CBP (Bowers et al., 2010), reduced acetylation of H3K122 by 80% (Figure 5D, compare lanes 9 and 10), indicating that H3K122ac is p300/CBP dependent. In contrast, C646 only slightly reduced (by ~30%) the TIP60-mediated acetylation of H2AK5ac (Kimura and Horikoshi, 1998) (Figure 4B).

(C) H3K122ac is enriched on the histone variant H3.3. Histones from HEK293 cells stably expressing HA/FLAG-tagged histone H3.1 and H3.3 were affinity purified with anti-FLAG beads and probed for H3K122ac, H3K9me3, and HA (as loading control) (left).

(D) Snapshot from UCSC browser showing normalized reads for different histone marks reveals peak-like distribution of H3K122ac enrichment.

(E) H3K122ac peaks are enriched at TSS. The genomic distribution of H3K122ac peaks was plotted according to their distance to RefSeq TSS (left pie chart); a random distribution of peaks of similar size (expected) is shown for comparison (right).

(F) UCSC browser snapshot showing the distribution of normalized reads at the TSS of two promoters for the indicated histone marks.

(G) The enrichment of H3K122ac at TSS correlates with gene expression levels. Shown is the normalized tag count for H3K122ac and other marks in 20 bp bins in a window ±2 kb from all RefSeq TSS. Q1 represents the quartile of genes with the lowest level of expression (blue), and Q4 represents the highest level of expression (red), respectively.

(H) Correlation of H3K122ac enrichment with other marks at TSS. Scatterplots showing the correlation between H3K122ac reads and reads of other marks at TSS as indicated.

See Figure S2 for preparation of mononucleosomes and validation of ChIP-seq experiments.

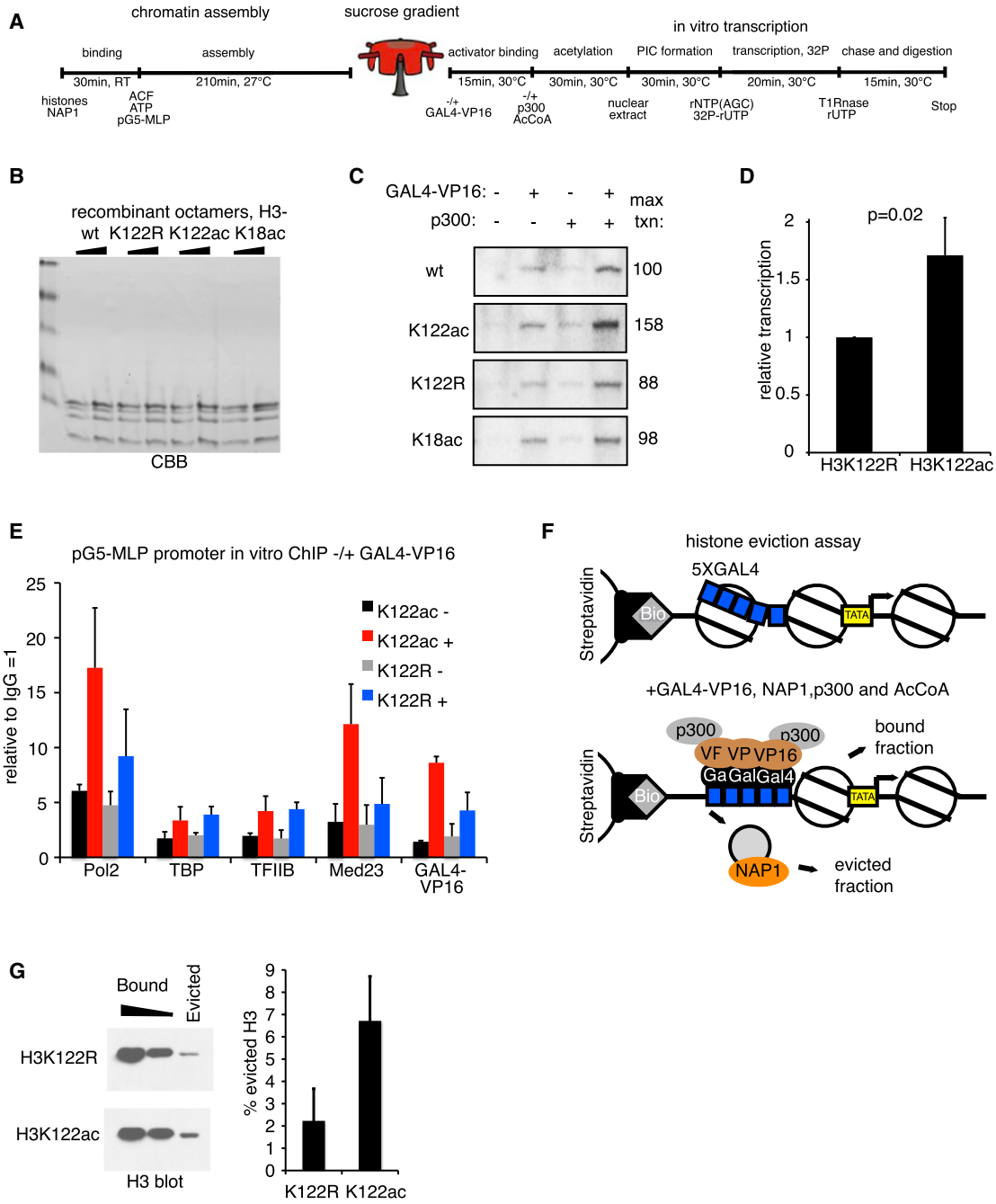

Figure 3. H3K122ac Stimulates Transcription of In-Vitro-Assembled Chromatin

(A) Schematic summary of the chromatin assembly and in vitro transcription assay. For details, see Extended Experimental Procedures.

(B) Purity and stoichiometry of recombinant histone octamers refolded with either WT H3, H3K122R, H3K122ac, or H3K18ac histones (see also Figure S3A) and analyzed by SDS-PAGE and CBB staining.

(C) In vitro transcription of chromatin is stimulated by H3K122ac. 20 ng sucrose gradient-purified chromatin was transcribed in the presence of AcCoA, ±20 ng GAL4-VP16 activator, and ±40 ng p300 as indicated. The recovered RNA was analyzed by denaturing PAGE and quantified relative to H3 WT (set as 100).

(D) Quantification of maximum transcription from H3K122ac chromatin in the presence of GAL4-VP16 and p300 was normalized to transcription from H3K122R control chromatin. Shown is the average ±SD of four experiments from two different preparations of chromatin. There is a significant difference in transcription ($p = 0.02$) calculated by two-tailed t test.

(E) In vitro ChIP assay for PIC components on H3K122ac and H3K122R chromatin. In vitro ChIP assay was carried out as IVT reaction in the presence of p300/AcCoA and ±GAL4-VP16 but was crosslinked after the PIC formation step (Figure 3A) for subsequent ChIP. The enrichment of different factors at the pG5-MLP promoter relative to IgG is shown as average ±SD of three replicates.

(legend continued on next page)

p300/CBP Acetylate H3K122 In Vitro and In Vivo

To demonstrate that p300 can indeed catalyze H3K122 acetylation, we performed in vitro HAT assays with human recombinant enzymes representing the three main classes of HATs: pCAF (GNAT family), MOF (MYST family), and p300 (orphan class) (Figure 4C). Among these enzymes, only p300 (and the paralog HAT CBP, see Figure S4D) acetylated H3K122 in our in vitro assays. The specificity of the H3K122ac antibody in these in vitro assays is demonstrated in Figure S4E. Interestingly, p300 acetylates H3K122 in vitro more efficiently on free histone octamers than on recombinant chromatin when compared to H3K18 in the tail, for example (Figures S4F and S4G). Though this explains why we detected little difference in transcription between fully assembled WT chromatin and H3K122R chromatin in the in vitro transcription assay, it is possible that, in vivo, other factors might promote H3K122 acetylation on chromatin (see Discussion).

Next, we asked whether p300 also acetylates H3K122 in vivo. Only the combined knockdown of p300 and CBP (Figures S4H and S4I) strongly reduced H3K122ac (Figure 4D), which can be explained by the overlapping substrate specificity of both enzymes in vivo (Jin et al., 2011). In line with this, transfected cells expressing p300 display a clearly elevated H3K122ac signal in comparison to cells transfected with green fluorescent protein (GFP) control alone (Figure 4E). Together, these experiments demonstrate that p300/CBP acetylate H3K122 in vitro and in vivo.

H3K122ac Marks ERα Binding Sites that Are Active Enhancers

Although we found that H3K122ac is highly enriched at TSS, 57% of all H3K122ac peaks locate distal to annotated TSS (Figure 2E). Interestingly, 78% of these distal peaks map to DNase-I-hypersensitive sites (DHS) (Figure 5A) and display significantly higher H3K122ac levels than distal peaks outside of DHS (Figure 5B), indicating enrichment of H3K122ac at distal regulatory elements such as enhancers. p300 enrichment has been established as a key signature of active enhancers (Visel et al., 2009). We therefore performed p300 ChIP-seq in MCF-7 cells (Figure S5A) and found that H3K122ac strongly enriches at distal DHS regions that are bound by p300 and, hence, are most likely enhancer regions (Figure 5C). Furthermore, we found that H3K122ac enrichment at DHS also strongly correlates with H3K27ac (Figures 5D and 5E), a known marker of active enhancers, but correlates only modestly with H3K4me1 (Figure 5E), a mark associated with both inactive (or potentially "poised") and active enhancers (Creyghton et al., 2010). Interestingly, despite a strong correlation between H3K27ac and H3K122ac at DHS, we observed differences in the enrichment of both marks around binding sites for specific transcription factors (Figure S5B), suggesting both overlapping and specific functions for H3K122ac and H3K27ac. H3K122ac therefore qualifies as a chromatin signature of active enhancers.

In MCF-7 cells, 96% of all ERα binding sites (ERBS) are located distal from TSS (Carroll et al., 2006). As observed for DHS, H3K122ac is strongly enriched at distal ERBS that are co-occupied by ERα and p300 (Figure S5C). We therefore used distal ERBS to further investigate a potential role for H3K122ac at enhancers. To test whether H3K122ac levels at ERBS are indeed functionally related to their enhancer activity, we made use of a genome-wide data set of distal ERBS that are actively engaged in long-range chromatin interactions (Fullwood et al., 2009). We found that H3K122ac is indeed more abundant at ERBS that are actively engaged in long-range chromatin interactions (Figure 5F), thus confirming the link between H3K122ac enrichment and enhancer function. Interestingly, H3K122ac levels increased not only at the promoter (Figure 4A) but also at a distal ERα enhancer of *TFF1(pS2)* upon activation by estrogen stimulation (Figure 5G). It has been described that enhancer activation coincides with transcription of enhancer-templated noncoding RNA (eRNA) (Kim et al., 2010; Wang et al., 2011), and we found that high H3K122ac levels at DHS correlate with significantly elevated eRNA transcript levels at enhancers (Figures 5G and S5D). H3K122ac might, therefore, not only directly stimulate transcription as shown in Figure 3 but potentially also facilitate enhancer activation.

Absence of H3K122ac Impairs Transcriptional Activation In Vivo

Having shown that H3K122ac can stimulate transcription in vitro and is strongly associated with genetic elements linked to active transcription, we next asked whether H3K122ac impacts on gene expression in vivo.

To this end, we took advantage of the power of yeast genetics that allowed us to replace endogenous WT H3 gene copies with a mutant H3 (which is so far not feasible in mammalian cells). Because of the higher homology of *Schizosaccharomyces pombe* to mammalian H3 (Figure S6A), we chose *S. pombe* over *Saccharomyces cerevisiae*. By using mass spectrometry, we established that H3K122ac occurs also in *S. pombe* (Figure S6B), indicating that this modification is highly conserved through evolution. We created *S. pombe* strains that express either WT histone H3 or histone H3K122R mutant from a single histone H3 gene. H3K122R mutant cells grew as well as WT cells (Figure S6D), demonstrating that the H3K122 to R mutation does not have an adverse effect on the general fitness. To assess the effect of H3K122ac on transcription, we monitored

(F) Schema of histone eviction assay from the biotin-labeled pG5-MLP promoter template (~620 bp) immobilized on streptavidin beads. The pG5-MLP promoter contains five GAL4 binding sites upstream of an adenoviral major late promoter (MLP). Nucleosomes are positioned randomly relative to the GAL4 binding sites (blue boxes) and the TATA box (yellow box). Histone eviction from the pG5-MLP template occurs only in the presence of GAL4-VP16, p300, NAP1, and AcCoA (Ito et al., 2000). NAP1 serves as histone acceptor and transfers histones from the linear template to a supercoiled acceptor plasmid (not shown).

(G) H3K122ac stimulates histone eviction. H3 content of the evicted and template-bound fractions from H3K122R and H3K122ac chromatin is shown on the left. The H3 content of evicted fractions was quantified densitometrically relative to the bound fraction from three replicates; shown is the average (±SD) from three replicates.

Additional controls for in vitro chromatin experiments, chromatin assembly, and IVT are shown in Figure S3.

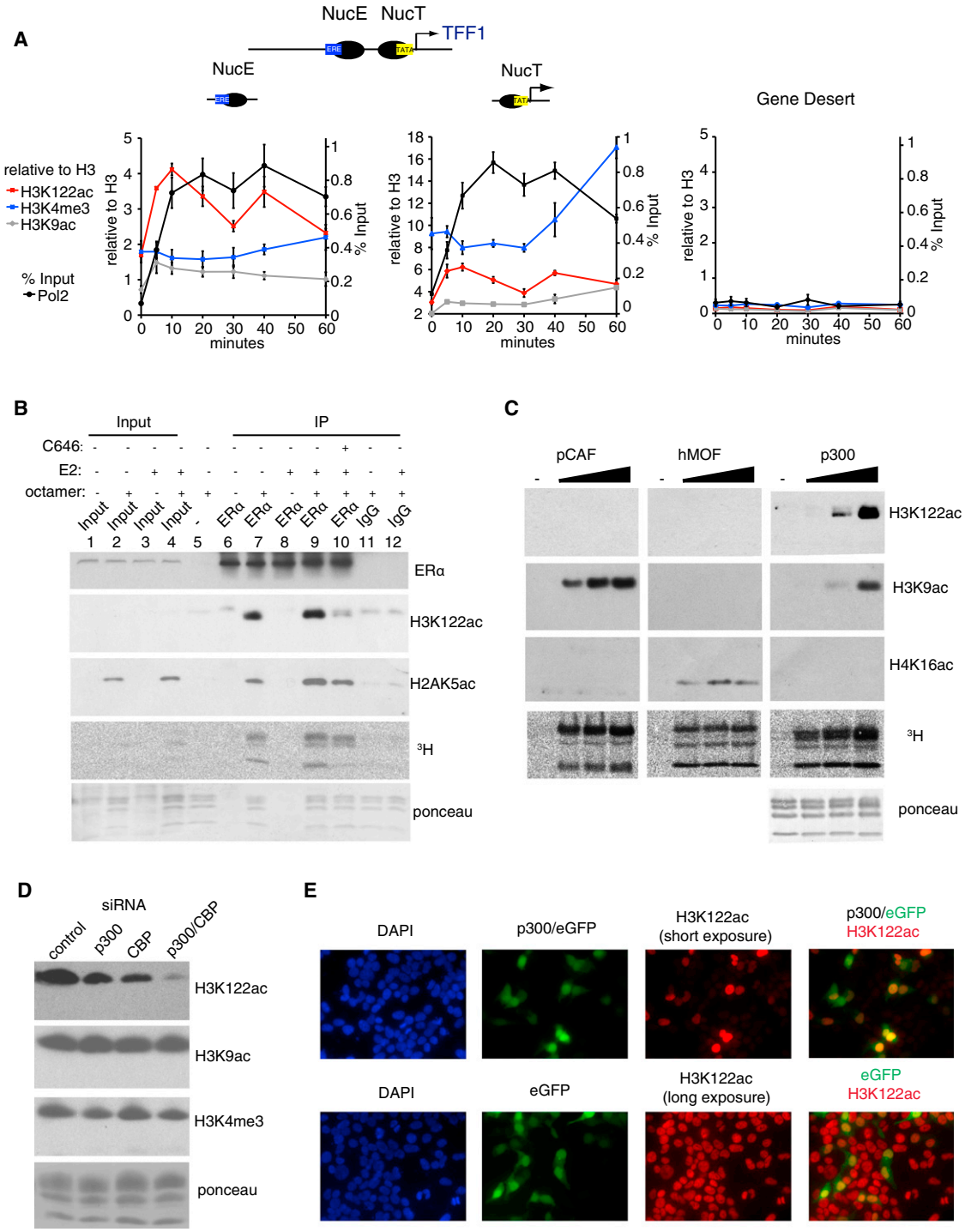

Figure 4. H3K122ac Levels Can Be Regulated by Estrogen Signaling via Recruitment of a p300/CBP-Dependent HAT Activity

(A) ChIP time course shows dynamics of H3K122ac at the *TFF1(pS2)* promoter. The graph on top shows the approximate position of the NucE (partially occupies an ERE, blue box) and NucT (partially occupies a TATA box, yellow box) relative to the TSS of *TFF1(pS2)*. ERα-dependent transcription of *TFF1(pS2)* was induced by E2/TPA (Sewack et al., 2001). Enrichment at NucE, NucT, and a control region (Gene Desert) is shown. H3K122ac, H3K9ac, and H3K4me3 enrichment was normalized to histone H3; RNA Pol II was plotted as % of input recovery. Data are shown as average (±SD) from two replicates.

(B) ERα recruits a p300/CBP-dependent HAT activity. MCF-7 nuclear extract was immunoprecipitated with ERα or IgG antibody in the absence or presence of estrogen. The IP on beads was used for an in vitro HAT assay (±25 μM C646, p300 inhibitor) and probed for HAT activity toward H3K122ac (second panel) and H2AK5ac (third panel). The slight reduction of H2AK5ac by C646 could be due to some p300 activity toward H2AK5 observed under in vitro conditions (Schiltz et al., 1999). ^{3}H incorporation (fourth panel) shows general HAT activity; Ponceau staining serves as loading control (bottom).

(legend continued on next page)

transcriptional activation of the *nmt1*+ gene (Maundrell, 1990) in WT and H3K122R cells (Figure 6A). Strikingly, although WT and H3K122R cells eventually reached the same steady-state *nmt1*+ mRNA levels, *nmt1*+ gene activation was severely delayed in the H3K122R mutant compared to a WT strain (Figures 6B and S6C). Thus, acetylation of H3K122 is important for rapid transcriptional gene activation in vivo.

DISCUSSION

The function of PTMs on the lateral surface of the histone octamer is thus far largely unknown. Among lateral surface modifications, acetylation of lysine is of particular interest because it neutralizes the positive charge of the lysine side chain and could thereby weaken ionic interactions between the basic lateral surface of the histone octamer and the negatively charged DNA backbone. Here, we have functionally characterized acetylation of H3K122 and revealed that, unlike a single H3 tail acetylation, H3K122 acetylation can be sufficient to stimulate transcription in vitro. We identify the coactivators p300/CBP as enzymes catalyzing H3K122ac and show that H3K122ac is specifically enriched at active TSS and enhancers as well as on H3.3- and H2A.Z-containing nucleosomes. In MCF-7 cells, H3K122ac is dynamically regulated at estrogen-regulated genes and marks enhancers that are actively engaged in transcriptional regulation. Finally, we show that mutation of H3K122 can impair transcriptional activation in vivo. We propose a model for H3K122ac on the lateral surface as a regulator of nucleosome function in transcription and as a signaling effector on chromatin (Figure 7).

It has been shown in vitro that chromatin with native, hyperacetylated histones is transcribed at higher rates than chromatin containing hypoacetylated histones (Li et al., 2010; Nightingale et al., 1998; Sheridan et al., 1997), demonstrating that histone acetylation not only correlates with sites of transcription in vivo but functionally contributes to it. The role of specific sites of histone acetylation for this transcriptional stimulation has so far been investigated for residues within the histone tails, either by deleting complete tails (An et al., 2002), by mutating lysine residues to arginines (K→R) that cannot be acetylated (An et al., 2004; Luebben et al., 2010), or by introducing lysine to glutamine (K→Q) mutations to mimic an acetylated lysine (Bintu et al., 2012). Although point mutants of histone residues are a good (and, in vivo, the only) strategy to address the function of histone modifications, it is unclear whether mutations fully reflect the properties of modified lysine residues. We therefore assembled chromatin with recombinant histones that carry single, site-specific acetylation at H3K122 and demonstrated that acetylation of H3K122 can be sufficient to stimulate transcription. This demonstrates that a single, site-specific acetylation on H3 increases transcription of a chromatinized DNA template.

How does H3K122ac stimulate transcription? According to the "histone code" hypothesis (Strahl and Allis, 2000), histone modifications may recruit binding proteins that, in turn, activate transcription. Recently, this has been elegantly demonstrated in vitro for H3K4me3, which recruits CHD1 to chromatin and thereby stimulates transcription (Lin et al., 2011). However, because we failed to identify a H3K122ac-specific binding protein using an unbiased SILAC (stable isotope labeling with amino acids in cell culture) approach (data not shown) and because H3K122 did not change chromatin compaction in a detectable manner (Figure S3D and data not shown), a direct effect of H3K122ac on histone-DNA binding and histone eviction is our preferred model for transcriptional stimulation by H3K122ac. Our conclusion that H3K122ac directly impacts histone-DNA binding in the dyad axis and is therefore mechanistically very different from histone tail modifications is supported by the finding that H3K122ac contributes to an increased rate of nucleosome disassembly upon mechanical stress in vitro (Simon et al., 2011).

Additionally, we found that H3K122ac co-occurs with the histone variants H3.3 and H2A.Z. The combination of H3.3 and H2A.Z at the TSS of transcribed genes renders nucleosomes "unstable" in vivo (Jin and Felsenfeld, 2007; Jin et al., 2009). Considering our in vitro data and the global correlation between H3K122ac and H3.3/H2A.Z, it is reasonable to assume that H3K122ac contributes to the instability of H3.3/H2A.Z nucleosomes at the TSS in vivo. In support of this, we observe a global depletion of nucleosomes at H3K122ac peaks (Figure S2E), suggesting that H3K122ac might indeed function by reducing nucleosomal density.

We show that H3K122ac is dependent on p300 and CBP in vitro and in vivo. Interestingly, H3K122 is only poorly acetylated by p300 in recombinant chromatin when compared to free histone octamers as a substrate. However, in the context of native chromatin in vivo, the presence of additional modifications, the specific recruitment of p300 and/or cofactors might directly stimulate the activity of p300 (Hyndman et al., 2012; Reynoird et al., 2010) or increase the rate of local unwrapping of nucleosomal DNA (Andrews and Luger, 2011; Koopmans et al., 2009), making H3K122 more accessible. Because H3K122ac is enriched at sites subject to high histone turnover, it is possible that in vivo H3K122 might become acetylated also in transitory states at TSS and enhancers.

Transcription in eukaryotes is often controlled by distal regulatory elements such as enhancers. Functional enhancers have

(C) p300 acetylates H3K122 in vitro. An in vitro HAT assay with recombinant histone octamers and increasing amounts of pCAF, MOF, and p300 (CBP see Figure S4C) is shown. HAT activity was monitored by autoradiography (^{3}H incorporation) and residue-specific activity with H3K9ac-, H4K16ac-, and H3K122ac-specific antibodies.

(D) Knockdown of p300/CBP reduces H3K122ac levels in vivo. MCF-7 cells were transfected with control or p300- and/or CBP-specific siRNA (see Figure S4H) and were analyzed for different histone modifications 72 hr after transfection by immunoblotting with antibodies as indicated. Ponceau staining shows equal loading.

(E) Overexpression of p300 increases H3K122ac in vivo. HEK293 cells were cotransfected with CMV-p300 and pEGFP-N1 plasmid DNA (top) or pEGFP-N1 alone (bottom). The DNA was stained with DAPI, transfected cells were detected by enhanced GFP (eGFP) expression (green), and the H3K122ac signal was detected with the H3K122ac antibody (red). The longer exposure of control transfected cells (bottom) shows endogenous H3K122ac signal.

For ERα-ChIP and additional HAT assays, see Figure S4. Primers are listed in Table S2.

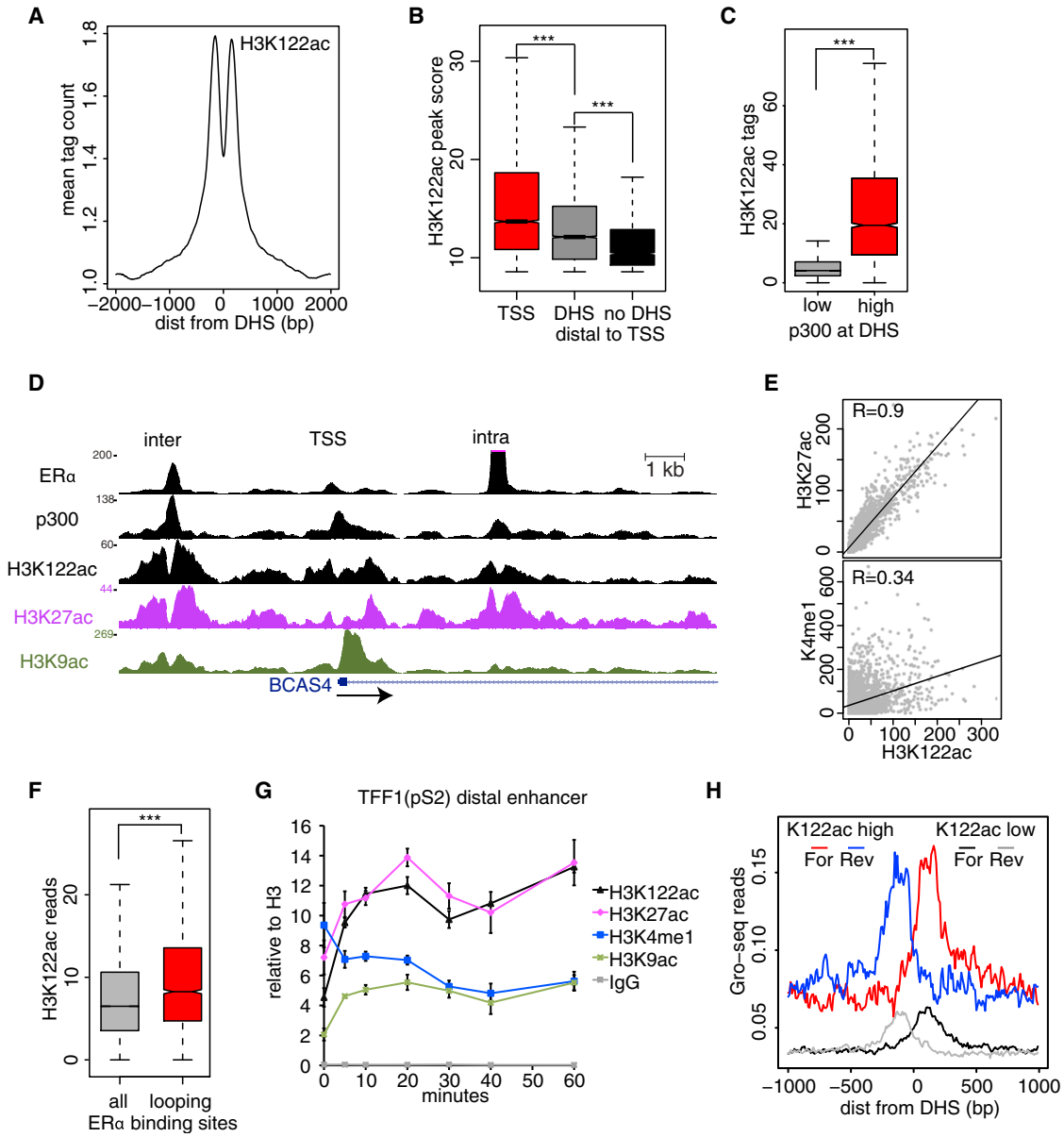

Figure 5. H3K122ac Marks Active Enhancer

(A) H3K122ac is enriched at DHS. The mean tag count of H3K122ac was plotted in a window ±2 kb around all DHS.

(B) Distal H3K122ac peaks mapping to DHS show higher H3K122ac enrichment than remaining distal peaks. Box plots show a statistical significant difference ($p < 2.2 \times 10^{-16}$) in the peak score of H3K122ac between TSS, distal peaks within DHS and distal peaks outside of DHS.

(C) H3K122ac is highly enriched at DHS co-occupied by p300. Box plot shows statistical significant difference ($p < 2.2 \times 10^{-16}$) in the tag count of H3K122ac at DHS with (red) or without (gray) high p300 co-occupancy.

(D) Snapshot showing reads for ERα, p300, H3K122ac, H3K27ac, and H3K9ac at the BCAS4 locus. Note enrichment of H3K122ac and H3K27ac at TSS and at two distal sites (inter- and intragenic) that are co-occupied by ERα and p300.

(E) Scatterplots showing the correlation of H3K27ac (high correlation) and H3K4me1 (modest correlation) reads with H3K122ac reads at DHS.

(F) H3K122ac is enriched at ERBS that loop to other genomic loci. The box plot shows statistical significant difference ($p < 1.5 \times 10^{-5}$) between normalized reads of H3K122ac at ERBS without (gray) or with physical interaction with other genomic locations (red).

(G) ChIP time course showing induction of H3K122ac upon activation of the distal *TFF1(pS2)* enhancer. MCF-7 cells were stimulated as in Figure 4A. Shown is enrichment of H3K122ac, H3K27ac, H3K9ac, H3K4me1, and IgG control relative to H3 ChIP. Data are average (±SD) from two replicates.

(H) Enhancers with high levels of H3K122ac transcribe high levels of eRNA. Aggregation plots show normalized GRO-seq reads at enhancers (DHS + p300) with low H3K122ac (black and gray line for + and − strands) or high H3K122ac enrichment (blue and red line for + and − strands).

Figure S5 contains additional data for p300 ChIP-seq and siRNA knockdown. Primers are listed in Table S2.

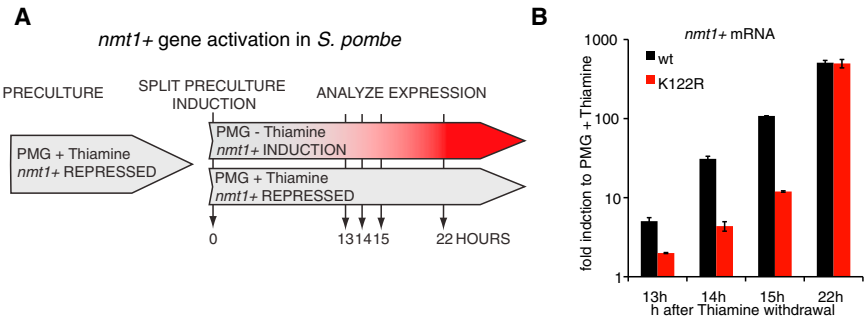

Figure 6. Role of H3K122ac in Transcription In Vivo

(A) *nmt1+* gene activation assay. Scheme showing the experimental setup of the *nmt1+* gene activation assay. A preculture (PMG + thiamine) was grown to fully repress the *nmt1+* gene. The culture was split and either grown in PMG without thiamine (induction of the *nmt1+* gene) or with thiamine (*nmt1+* repressed). Expression was analyzed 13, 14, 15, and 22 hr after induction.

(B) H3K122R mutant strain shows slower *nmt1+* gene activation kinetics. The time course of activation of the *nmt1+* gene in the H3K122R mutant, which lacks H3K122 acetylation, and H3 WT control cells. The fold induction is expressed as a ratio of *nmt1+* RNA levels under induced conditions (PMG) relative to repressed conditions (PMG + thiamine) at each time point. The average is shown from three technical replicates (±SD) of a representative experiment.

Figure S6 contains a clustalW alignment, a spectra of H3K122ac peptides from *S. pombe*, and additional data on the *nmt1+* time course. Primers are listed in Table S1.

been predicted genome wide by binding of p300, the presence of H3K4me1 and H3K27ac, and the absence of H3K4me3 (Heintzman et al., 2007; Rada-Iglesias et al., 2011; Visel et al., 2009). We found that, in MCF7 cells, H3K122ac is not only enriched at the TSS of transcribed genes but is also enriched at active enhancers bound by p300 and ERα. This suggests that using H3K122ac as a criterion to identify enhancers could further increase the robustness of enhancer prediction based on chromatin features. Although histone marks have been successfully used to identify enhancers, surprisingly little is known regarding their function at these sites. Based on the observation that H3K122ac increases activator binding and transcription in vitro, we speculate that H3K122ac could facilitate binding of regulatory factors to enhancers and/or the transcription of eRNA in vivo.

A Regulated Nucleosome Mobility Model for the Function of Lateral Surface Acetylations

Most previously studied histone modifications are located within the flexible tails of histones, and our understanding of their mechanistic impact on chromatin-based processes is still limited. A quantitative biophysical model (Fenley et al., 2010) predicts that, in contrast to tail modifications, even a slight decrease in the charge on the lateral surface (e.g., by H3K122

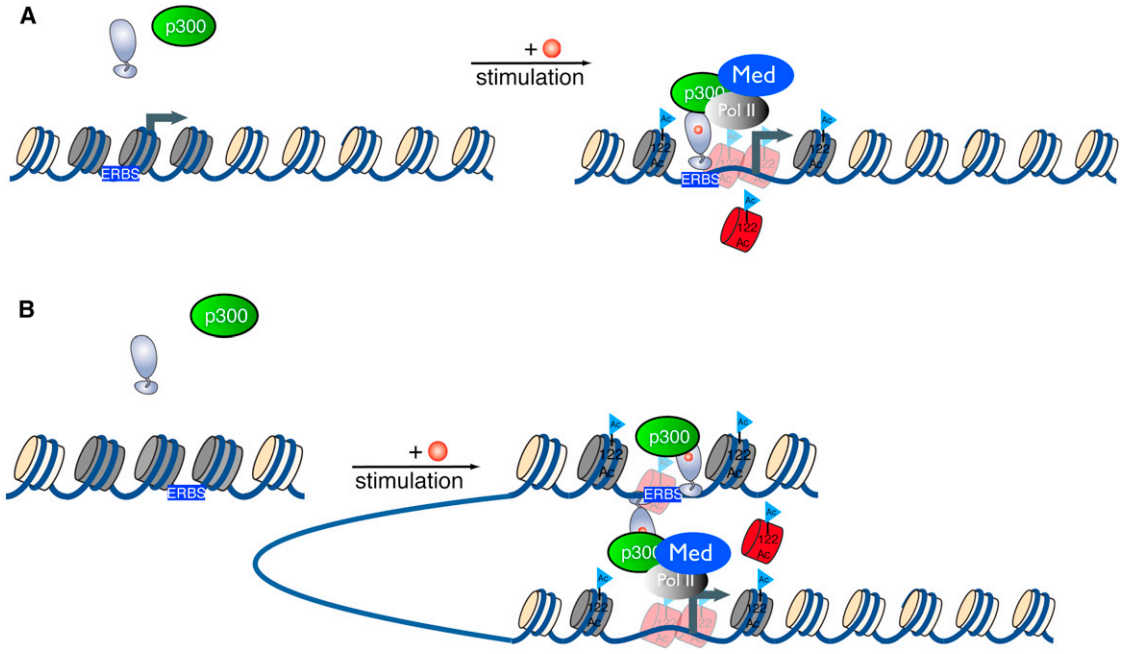

Figure 7. Model for the Regulation and Function of H3K122ac in Transcriptional Activation

(A and B) Recruitment of p300 to chromatin, for example by ERα (gray), to promoter-proximal ERBS (blue box) (A) or distal ERBS (B) in the presence of estrogen locally induces H3K122ac (blue flags). H3K122ac then stimulates histone eviction, presumably from H2A.Z(ac)- or H3.3/H2A.Z-containing nucleosomes (gray octamers) that are enriched at TSS (A) and enhancers (B). H3K122ac-stimulated histone eviction enhances further recruitment of additional factors, including mediator (Med) and Pol II, and thereby stimulates transcription.

acetylation) can have a direct effect on nucleosome mobility. Our in vitro results that H3K122ac can promote histone eviction and transcription, as well as our in vivo findings that H3K122ac is present at genomic regions with a role in transcription, fully support a regulation of nucleosome mobility by lateral surface modifications. Finally, our data from *S. pombe* strongly suggest that the role of H3K122 in transcription is evolutionarily conserved. This is further supported by H3K122 mutants in *S. cerevisiae* that result in transcriptional derepression (Hyland et al., 2005) and in a decrease in nucleosome density in highly transcribed genes (Hainer and Martens, 2011).

Importantly, besides H3K122, other lysines on the lateral surface of H3—in particular, H3K56, H3K64, and H3K115 (Tropberger and Schneider, 2010)—can also be modified and might act synergistically and/or in different combinations, increasing the impact on nucleosome dynamics. Additionally, phosphorylation on the lateral surface (e.g., at H3T118) could have a similar effect in reducing the DNA-binding affinity. As our work demonstrates, modifications on the lateral surface of the nucleosome are of central importance for chromatin biology, and we are just beginning to understand their mechanism of action and their role in the regulation of transcription.

EXPERIMENTAL PROCEDURES

Cell Culture

MCF-7 cells were kindly provided by Kartiki V. Desai and were cultured under standard conditions. For details on culture and stimulation of cells used throughout this study, see Extended Experimental Procedures.

Immunoblot Analysis of Histones

Histones were separated by Tricine-based SDS-PAGE (Schägger and von Jagow, 1987) and transferred to nitrocelluose membrane (BA79, Whatman). Membranes were blocked in TBST (0.2% Tween-20) with 4% BSA. For detection of H3K122ac, the antibody was diluted 1:800 in TBST 4% BSA at 4°C overnight (O/N). For a complete list of antibodies, see Extended Experimental Procedures.

Immunofluorescence Analysis

For immunofluorescence analysis, cells were cultured on poly-L-lysine (Sigma) -coated glass coverslips and stained with DAPI and the H3K122ac antibody in a 1:100 dilution as described in detail in Daujat et al. (2009).

Histone Acetyltransferase Assay

Recombinant p300 was purified from baculovirus-infected Sf9 cells as described (Kraus and Kadonaga, 1998). Recombinant human MOF was a gift from Herbert Holz. HAT assays were performed at 30°C for 60 min as described in Extended Experimental Procedures.

Mononucleosome IP

Native mononucleosomes were prepared by micrococcal nuclease digestion of MCF-7 cells as described (Wagschal et al., 2007). Mononucleosomes were purified by sucrose gradient centrifugation and immunoprecipitated with the H3K122ac antibody as outlined in Extended Experimental Procedures.

ChIP

For ChIP-seq of H3K122ac, H3K27ac, H2A.Z, and H2A.Zac, chromatin was prepared by micrococcal nuclease digestion of crosslinked MCF-7 nuclei. For p300, ERα, and the ChIP time course, cells were crosslinked with formaldehyde and sonicated in a Bioruptor (Diagenode). Detailed protocols are provided in Extended Experimental Procedures. Primers used for qPCR analysis with ABsolute qPCR SYBR Green Mix (Abgene) on an Applied Biosystems 7300 real-time PCR system are listed in Tables S1, S2, and S3.

ChIP-Seq Analysis

ChIP-seq libraries were prepared according to manufacturer's protocols and sequenced with Illumina GAII. The raw data were processed using the Solexa Pipeline and mapped to the reference genome (NCBI Build 36, hg18) using Eland (Illumina) or Bowtie2 (Langmead and Salzberg, 2012). For details on libraries used throughout this study, see Table S4; for details on peak calling (Table S5) and bioinformatics analysis, see Extended Experimental Procedures.

In Vitro Assays with Recombinant Chromatin

Briefly, histones with or without acetylation were expressed recombinantly in *E. coli* as described (Neumann et al., 2009) and refolded into histone octamers (Luger et al., 1999). Recombinant chromatin was assembled by NAP1 and ACF (Ito et al., 1997), and in vitro transcription of purified recombinant chromatin was performed as described (Margueron et al., 2008). For histone eviction assays, chromatin was assembled by step-wise salt dialysis. Detailed protocols for all in vitro methods (transcription, ChIP, and histone eviction) are provided in Extended Experimental Procedures.

S. pombe Strains and Experiments

The H3K122R mutant strain was created as described in Mellone et al. (2003). Details about *S. pombe* strains used in this study are listed in Table S6. For the *nmt1*+ induction experiments, equal numbers of yeast from different strains were transferred to media supplemented with or without thiamine and mRNA analyzed by quantitative RT-PCR (qRT-PCR) at the time points indicated. Details on the *nmt1*+ induction experiments are provided in the Extended Experimental Procedures.

ACCESSION NUMBERS

ChIP-seq data were deposited in GEO under the accession number GSE35954.

SUPPLEMENTAL INFORMATION

Supplemental Information includes Extended Experimental Procedures, six figures, and six tables and can be found with this article online at http://dx.doi.org/10.1016/j.cell.2013.01.032.

ACKNOWLEDGMENTS

We thank S. Daujat and all members of the Schneider and Margueron laboratories. We are grateful to H. Neumann for providing expression plasmids and advice and to G. Längst for ACF remodeling complex. We would like to thank I. del Valle for cell pellets for histone extraction. We thank H. Holz for advice and help for protein purification and M. Cohen for quantification of acetylated peptides. Work in the Schneider laboratory was supported by the Max Planck Society, the DFG (through SFB 746), the Fondation pour la Recherche Medicale, and an ERC starting grant; the R. Margueron laboratory was supported by the Institut Nationale du Cancer and Fondation pour la Recherche Medicale. Research in the laboratory of M. Bühler was supported by funds from the Swiss National Science Foundation, the ERC, the Gebert Rüf Foundation, the Novartis Research Foundation, and the EMBO Young Investigator Programme.

Received: April 4, 2012
Revised: November 25, 2012
Accepted: January 22, 2013
Published: February 14, 2013

REFERENCES

An, W., Palhan, V.B., Karymov, M.A., Leuba, S.H., and Roeder, R.G. (2002). Selective requirements for histone H3 and H4 N termini in p300-dependent transcriptional activation from chromatin. Mol. Cell *9*, 811–821.

An, W., Kim, J., and Roeder, R.G. (2004). Ordered cooperative functions of PRMT1, p300, and CARM1 in transcriptional activation by p53. Cell *117*, 735–748.

Andrews, A.J., and Luger, K. (2011). Nucleosome structure(s) and stability: variations on a theme. Annu. Rev. Biophys. *40*, 99–117.

Ausio, J., Dong, F., and van Holde, K.E. (1989). Use of selectively trypsinized nucleosome core particles to analyze the role of the histone "tails" in the stabilization of the nucleosome. J. Mol. Biol. *206*, 451–463.

Bannister, A.J., and Kouzarides, T. (2011). Regulation of chromatin by histone modifications. Cell Res. *21*, 381–395.

Barski, A., Cuddapah, S., Cui, K., Roh, T.Y., Schones, D.E., Wang, Z., Wei, G., Chepelev, I., and Zhao, K. (2007). High-resolution profiling of histone methylations in the human genome. Cell *129*, 823–837.

Bintu, L., Ishibashi, T., Dangkulwanich, M., Wu, Y.-Y., Lubkowska, L., Kashlev, M., and Bustamante, C. (2012). Nucleosomal elements that control the topography of the barrier to transcription. Cell *151*, 738–749.

Bowers, E.M., Yan, G., Mukherjee, C., Orry, A., Wang, L., Holbert, M.A., Crump, N.T., Hazzalin, C.A., Liszczak, G., Yuan, H., et al. (2010). Virtual ligand screening of the p300/CBP histone acetyltransferase: identification of a selective small molecule inhibitor. Chem. Biol. *17*, 471–482.

Carroll, J.S., Meyer, C.A., Song, J., Li, W., Geistlinger, T.R., Eeckhoute, J., Brodsky, A.S., Keeton, E.K., Fertuck, K.C., Hall, G.F., et al. (2006). Genome-wide analysis of estrogen receptor binding sites. Nat. Genet. *38*, 1289–1297.

Cocklin, R.R., and Wang, M. (2003). Identification of methylation and acetylation sites on mouse histone H3 using matrix-assisted laser desorption/ionization time-of-flight and nanoelectrospray ionization tandem mass spectrometry. J. Protein Chem. *22*, 327–334.

Cosgrove, M.S., Boeke, J.D., and Wolberger, C. (2004). Regulated nucleosome mobility and the histone code. Nat. Struct. Mol. Biol. *11*, 1037–1043.

Creyghton, M.P., Cheng, A.W., Welstead, G.G., Kooistra, T., Carey, B.W., Steine, E.J., Hanna, J., Lodato, M.A., Frampton, G.M., Sharp, P.A., et al. (2010). Histone H3K27ac separates active from poised enhancers and predicts developmental state. Proc. Natl. Acad. Sci. USA *107*, 21931–21936.

Daujat, S., Weiss, T., Mohn, F., Lange, U.C., Ziegler-Birling, C., Zeissler, U., Lappe, M., Schübeler, D., Torres-Padilla, M.-E., and Schneider, R. (2009). H3K64 trimethylation marks heterochromatin and is dynamically remodeled during developmental reprogramming. Nat. Struct. Mol. Biol. *16*, 777–781.

Fenley, A.T., Adams, D.A., and Onufriev, A.V. (2010). Charge state of the globular histone core controls stability of the nucleosome. Biophys. J. *99*, 1577–1585.

Freitas, M.A., Sklenar, A.R., and Parthun, M.R. (2004). Application of mass spectrometry to the identification and quantification of histone post-translational modifications. J. Cell. Biochem. *92*, 691–700.

Fullwood, M.J., Liu, M.H., Pan, Y.F., Liu, J., Xu, H., Mohamed, Y.B., Orlov, Y.L., Velkov, S., Ho, A., Mei, P.H., et al. (2009). An oestrogen-receptor-alpha-bound human chromatin interactome. Nature *462*, 58–64.

Garcia, B.A. (2009). Mass spectrometric analysis of histone variants and post-translational modifications. Front Biosci. (Schol. Ed.) *1*, 142–153.

Goldberg, A.D., Banaszynski, L.A., Noh, K.-M., Lewis, P.W., Elsaesser, S.J., Stadler, S., Dewell, S., Law, M., Guo, X., Li, X., et al. (2010). Distinct factors control histone variant H3.3 localization at specific genomic regions. Cell *140*, 678–691.

Hainer, S.J., and Martens, J.A. (2011). Identification of histone mutants that are defective for transcription-coupled nucleosome occupancy. Mol. Cell. Biol. *31*, 3557–3568.

Hall, M.A., Shundrovsky, A., Bai, L., Fulbright, R.M., Lis, J.T., and Wang, M.D. (2009). High-resolution dynamic mapping of histone-DNA interactions in a nucleosome. Nat. Struct. Mol. Biol. *16*, 124–129.

Heintzman, N.D., Stuart, R.K., Hon, G., Fu, Y., Ching, C.W., Hawkins, R.D., Barrera, L.O., Van Calcar, S., Qu, C., Ching, K.A., et al. (2007). Distinct and predictive chromatin signatures of transcriptional promoters and enhancers in the human genome. Nat. Genet. *39*, 311–318.

Hyland, E.M., Cosgrove, M.S., Molina, H., Wang, D., Pandey, A., Cottee, R.J., and Boeke, J.D. (2005). Insights into the role of histone H3 and histone H4 core modifiable residues in Saccharomyces cerevisiae. Mol. Cell. Biol. *25*, 10060–10070.

Hyndman, B.D., Thompson, P., Bayly, R., Côté, G.P., and Lebrun, D.P. (2012). E2A proteins enhance the histone acetyltransferase activity of the transcriptional co-activators CBP and p300. Biochim. Biophys. Acta *1819*, 446–453.

Ito, T., Bulger, M., Pazin, M.J., Kobayashi, R., and Kadonaga, J.T. (1997). ACF, an ISWI-containing and ATP-utilizing chromatin assembly and remodeling factor. Cell *90*, 145–155.

Ito, T., Ikehara, T., Nakagawa, T., Kraus, W.L., and Muramatsu, M. (2000). p300-mediated acetylation facilitates the transfer of histone H2A-H2B dimers from nucleosomes to a histone chaperone. Genes Dev. *14*, 1899–1907.

Iwasaki, W., Tachiwana, H., Kawaguchi, K., Shibata, T., Kagawa, W., and Kurumizaka, H. (2011). Comprehensive structural analysis of mutant nucleosomes containing lysine to glutamine (KQ) substitutions in the H3 and H4 histone-fold domains. Biochemistry *50*, 7822–7832.

Jin, C., and Felsenfeld, G. (2007). Nucleosome stability mediated by histone variants H3.3 and H2A.Z. Genes Dev. *21*, 1519–1529.

Jin, C., Zang, C., Wei, G., Cui, K., Peng, W., Zhao, K., and Felsenfeld, G. (2009). H3.3/H2A.Z double variant-containing nucleosomes mark 'nucleosome-free regions' of active promoters and other regulatory regions. Nat. Genet. *41*, 941–945.

Jin, Q., Yu, L.-R., Wang, L., Zhang, Z., Kasper, L.H., Lee, J.-E., Wang, C., Brindle, P.K., Dent, S.Y.R., and Ge, K. (2011). Distinct roles of GCN5/PCAF-mediated H3K9ac and CBP/p300-mediated H3K18/27ac in nuclear receptor transactivation. EMBO J. *30*, 249–262.

Kim, T.K., Hemberg, M., Gray, J.M., Costa, A.M., Bear, D.M., Wu, J., Harmin, D.A., Laptewicz, M., Barbara-Haley, K., Kuersten, S., et al. (2010). Widespread transcription at neuronal activity-regulated enhancers. Nature *465*, 182–187.

Kimura, A., and Horikoshi, M. (1998). Tip60 acetylates six lysines of a specific class in core histones in vitro. Genes Cells *3*, 789–800.

Koopmans, W.J., Buning, R., Schmidt, T., and van Noort, J. (2009). spFRET using alternating excitation and FCS reveals progressive DNA unwrapping in nucleosomes. Biophys. J. *97*, 195–204.

Kouzarides, T. (2007). Chromatin modifications and their function. Cell *128*, 693–705.

Kraus, W.L., and Kadonaga, J.T. (1998). p300 and estrogen receptor cooperatively activate transcription via differential enhancement of initiation and reinitiation. Genes Dev. *12*, 331–342.

Krogan, N.J., Kim, M., Tong, A., Golshani, A., Cagney, G., Canadien, V., Richards, D.P., Beattie, B.K., Emili, A., Boone, C., et al. (2003). Methylation of histone H3 by Set2 in Saccharomyces cerevisiae is linked to transcriptional elongation by RNA polymerase II. Mol. Cell. Biol. *23*, 4207–4218.

Langmead, B., and Salzberg, S.L. (2012). Fast gapped-read alignment with Bowtie 2. Nat. Methods *9*, 357–359.

Li, G., Margueron, R., Hu, G., Stokes, D., Wang, Y.-H., and Reinberg, D. (2010). Highly compacted chromatin formed in vitro reflects the dynamics of transcription activation in vivo. Mol. Cell *38*, 41–53.

Lin, J.J., Lehmann, L.W., Bonora, G., Sridharan, R., Vashisht, A.A., Tran, N., Plath, K., Wohlschlegel, J.A., and Carey, M. (2011). Mediator coordinates PIC assembly with recruitment of CHD1. Genes Dev. *25*, 2198–2209.

Luebben, W.R., Sharma, N., and Nyborg, J.K. (2010). Nucleosome eviction and activated transcription require p300 acetylation of histone H3 lysine 14. Proc. Natl. Acad. Sci. USA *107*, 19254–19259.

Luger, K., Rechsteiner, T.J., and Richmond, T.J. (1999). Preparation of nucleosome core particle from recombinant histones. Methods Enzymol. *304*, 3–19.

Margueron, R., Li, G., Sarma, K., Blais, A., Zavadil, J., Woodcock, C.L., Dynlacht, B.D., and Reinberg, D. (2008). Ezh1 and Ezh2 maintain repressive chromatin through different mechanisms. Mol. Cell *32*, 503–518.

Maundrell, K. (1990). nmt1 of fission yeast. A highly transcribed gene completely repressed by thiamine. J. Biol. Chem. *265*, 10857–10864.

Mellone, B.G., Ball, L., Suka, N., Grunstein, M.R., Partridge, J.F., and Allshire, R.C. (2003). Centromere silencing and function in fission yeast is governed by the amino terminus of histone H3. Curr. Biol. *13*, 1748–1757.

Neumann, H., Hancock, S.M., Buning, R., Routh, A., Chapman, L., Somers, J., Owen-Hughes, T., van Noort, J., Rhodes, D., and Chin, J.W. (2009). A method for genetically installing site-specific acetylation in recombinant histones defines the effects of H3 K56 acetylation. Mol. Cell *36*, 153–163.

Nightingale, K.P., Wellinger, R.E., Sogo, J.M., and Becker, P.B. (1998). Histone acetylation facilitates RNA polymerase II transcription of the Drosophila hsp26 gene in chromatin. EMBO J. *17*, 2865–2876.

Owen-Hughes, T., and Workman, J.L. (1996). Remodeling the chromatin structure of a nucleosome array by transcription factor-targeted trans-displacement of histones. EMBO J. *15*, 4702–4712.

Perissi, V., and Rosenfeld, M.G. (2005). Controlling nuclear receptors: the circular logic of cofactor cycles. Nat. Rev. Mol. Cell Biol. *6*, 542–554.

Rada-Iglesias, A., Bajpai, R., Swigut, T., Brugmann, S.A., Flynn, R.A., and Wysocka, J. (2011). A unique chromatin signature uncovers early developmental enhancers in humans. Nature *470*, 279–283.

Reynoird, N., Schwartz, B.E., Delvecchio, M., Sadoul, K., Meyers, D., Mukherjee, C., Caron, C., Kimura, H., Rousseaux, S., Cole, P.A., et al. (2010). Oncogenesis by sequestration of CBP/p300 in transcriptionally inactive hyperacetylated chromatin domains. EMBO J. *29*, 2943–2952.

Ruthenburg, A.J., Li, H., Milne, T.A., Dewell, S., McGinty, R.K., Yuen, M., Ueberheide, B., Dou, Y., Muir, T.W., Patel, D.J., and Allis, C.D. (2011). Recognition of a mononucleosomal histone modification pattern by BPTF via multivalent interactions. Cell *145*, 692–706.

Schägger, H., and von Jagow, G. (1987). Tricine-sodium dodecyl sulfate-polyacrylamide gel electrophoresis for the separation of proteins in the range from 1 to 100 kDa. Anal. Biochem. *166*, 368–379.

Schiltz, R.L., Mizzen, C.A., Vassilev, A., Cook, R.G., Allis, C.D., and Nakatani, Y. (1999). Overlapping but distinct patterns of histone acetylation by the human coactivators p300 and PCAF within nucleosomal substrates. J. Biol. Chem. *274*, 1189–1192.

Sewack, G.F., and Hansen, U. (1997). Nucleosome positioning and transcription-associated chromatin alterations on the human estrogen-responsive pS2 promoter. J. Biol. Chem. *272*, 31118–31129.

Sewack, G.F., Ellis, T.W., and Hansen, U. (2001). Binding of TATA binding protein to a naturally positioned nucleosome is facilitated by histone acetylation. Mol. Cell. Biol. *21*, 1404–1415.

Sharma, N., and Nyborg, J.K. (2008). The coactivators CBP/p300 and the histone chaperone NAP1 promote transcription-independent nucleosome eviction at the HTLV-1 promoter. Proc. Natl. Acad. Sci. USA *105*, 7959–7963.

Sheridan, P.L., Mayall, T.P., Verdin, E., and Jones, K.A. (1997). Histone acetyltransferases regulate HIV-1 enhancer activity in vitro. Genes Dev. *11*, 3327–3340.

Simon, M., North, J.A., Shimko, J.C., Forties, R.A., Ferdinand, M.B., Manohar, M., Zhang, M., Fishel, R., Ottesen, J.J., and Poirier, M.G. (2011). Histone fold modifications control nucleosome unwrapping and disassembly. Proc. Natl. Acad. Sci. USA *108*, 12711–12716.

Strahl, B.D., and Allis, C.D. (2000). The language of covalent histone modifications. Nature *403*, 41–45.

Tan, M., Luo, H., Lee, S., Jin, F., Yang, J.S., Montellier, E., Buchou, T., Cheng, Z., Rousseaux, S., Rajagopal, N., et al. (2011). Identification of 67 histone marks and histone lysine crotonylation as a new type of histone modification. Cell *146*, 1016–1028.

Tropberger, P., and Schneider, R. (2010). Going global: Novel histone modifications in the globular domain of H3. Epigenetics *5*, 112–117.

Turner, B.M. (2000). Histone acetylation and an epigenetic code. Bioessays *22*, 836–845.

Valdés-Mora, F., Song, J.Z., Statham, A.L., Strbenac, D., Robinson, M.D., Nair, S.S., Patterson, K.I., Tremethick, D.J., Stirzaker, C., and Clark, S.J. (2012). Acetylation of H2A.Z is a key epigenetic modification associated with gene deregulation and epigenetic remodeling in cancer. Genome Res. *22*, 307–321.

Visel, A., Blow, M.J., Li, Z., Zhang, T., Akiyama, J.A., Holt, A., Plajzer-Frick, I., Shoukry, M., Wright, C., Chen, F., et al. (2009). ChIP-seq accurately predicts tissue-specific activity of enhancers. Nature *457*, 854–858.

Wagschal, A., Delaval, K., Pannetier, M., Arnaud, P., and Feil, R. (2007). Chromatin immunoprecipitation (ChIP) on unfixed chromatin from cells and tissues to analyze histone modifications. CSH Protoc. *2007*, pdb.prot4767.

Wang, D., Garcia-Bassets, I., Benner, C., Li, W., Su, X., Zhou, Y., Qiu, J., Liu, W., Kaikkonen, M.U., Ohgi, K.A., et al. (2011). Reprogramming transcription by distinct classes of enhancers functionally defined by eRNA. Nature *474*, 390–394.

Workman, J.L., and Kingston, R.E. (1992). Nucleosome core displacement in vitro via a metastable transcription factor-nucleosome complex. Science *258*, 1780–1784.

Zhang, L., Eugeni, E.E., Parthun, M.R., and Freitas, M.A. (2003). Identification of novel histone post-translational modifications by peptide mass fingerprinting. Chromosoma *112*, 77–86.

Zhou, V.W., Goren, A., and Bernstein, B.E. (2010). Charting histone modifications and the functional organization of mammalian genomes. Nat. Rev. Genet. *12*, 7–18.

EXTENDED EXPERIMENTAL PROCEDURES

Antibodies

The H3K122ac antibody is commercially available (Abcam ab33309), both lot #436839 and #802048 were successfully tested. Additional antibodies: general H3, ChIP only (Abcam ab1791) general H3, immunoblot only (Abcam ab10799), H3K9me3 (Upstate 07-442), H3K9ac, immunoblot only (Cell Signaling 9761), H3K18ac (Cell Signaling 9675), H3K27ac (Abcam ab4729) H3K27me3 (Upstate 07-449), H3K36me3 (Diagenode pAB-058-050), H3K56ac (Epitomics 2134-1), H3K4me3 (Diagenode pAb-003-050), H3K9ac, ChIP only (Abcam ab4441), H2A.Z (Millipore 07-594), H2A.Zac (Abcam ab18262), HA (12CA5), H4K16ac (Millipore 07-329), H3K4me1 (Abcam ab8895), IgG control (Millipore CS200851), polymerase 2 (Abcam ab5408), p300 (Santa Cruz sc-585), CBP (Santa Cruz sc-369), TFIIB (Millipore #06-243), estrogen receptor alpha (Santa Cruz sc-543). MED23 (BD PharMingen #550429) Monoclonal TBP and GAL4 antibodies were kindly provided by Laslo Tora.

Mammalian Cell Culture and Treatment

Cells were maintained at 37°C in a humidified atmosphere containing 5% CO_2. Michigan Cancer Foundation 7 cells (MCF-7, kindly provided by Dr. Kartiki Versai, Genome Institute of Singapore) were maintained in Dulbecco's modified Eagle's medium high glucose (DMEM, PAA) supplemented with 10% Fetal Bovine Serum (Perbio), 1% L-Glutamine (200 mM) and 1x Pen/Strep solution (PAA). Prior to stimulation with 17b-estradiol (E2, Sigma), MCF-7 cells were hormone-starved in phenol red-free DMEM (Sigma) supplemented with 2.5% charcoal-dextran stripped FBS (Sigma) and 200mM L-glutamine and 1x Pen/Strep solution (PAA) for three days. MCF-7 cells were stimulated with 10nM E2, 100nM TPA or equal volume of vehicle (DMSO). Human Embryonic Kidney (HEK293) cells stably expressing HA/FLAG-H3.1 or -H3.3 were cultured in DMEM supplemented with 10% Fetal Bovine Serum (Perbio), 200mM L-glutamine and 1x Pen/Strep solution (PAA) and 750μg/ml G418. HeLa S3 cells were kindly provided by Gerhard Mittler and maintained in RPMI media supplemented with 10% FCS (PAA), 200mM L-glutamine and 1x Pen/Strep solution (PAA).

Transient Transfection of Eukaryotic Cells

Predesigned (ON-TARGETplus SMARTpool) short interfering RNAs (siRNAs) specific for *CBP* (L-003477-00-0005), *p300* (L-003486-00-0005), *pCAF* (L-005055-00-005), *GCN5* (L-009722-00-005) and a nontargeting negative control siRNA (D-001810-01-05) were purchased from Dharmacon. The siRNAs were transfected with Lipofectamine RNAiMAX (Invitrogen) transfection reagent. The transfection was carried out based on the "Reverse Transfection" protocol provided by Invitrogen. siRNAs were transfected with a final concentration of: CBP 10nmol, p300 25nmol, pCAF 25nmol, GCN5 50nmol, control 35nmol (p300/CBP) or 75nmol (pCAF/GCN5).

For p300 overexpression HEK293 cells were transfected with pCMVb-p300-HA by lipofection using FuGene HD transfection reagent (Roche) according to the manufactures instructions.

Plasmids

pAcKRS-3 and pCDF PylT-1 were kindly provided by Jason Chin and are described in (Neumann et al., 2009). Human H3 was cloned into the NcoI-XhoI restriction sites of pCDF PylT-1 to express untagged H3. H3K122R, H3K122amber and H3K18amber mutants were introduced by PCR-mediated mutagenesis. Pet21a-H2A, pet21a-H2B and pet21a-H4 for histone expression were kindly provided by JD Parvin.

H3.1 and H3.3 with a C-terminal HA/FLAG tag were expressed from pFP-N1-H3.1-HA/FLAG and pFP-N1-H3.3-HA/FLAG, respectively: First the CMV promoter of pFP-N1-eGFP (gift from K. Hammerschmidt) was replaced with an elongation factor 1a promoter (AseI-NheI). Next human H3.1 and H3.3 were cloned with a HA/FLAG-tag into the HindIII-BamHI restriction sites. pG5-MLP plasmid for in vitro transcription was provided by Guohong Li.

Mass Spectrometry: MS/MS Analysis of Acetylated H3

In vivo modified histone H3 was acid extracted from MCF-7 and mouse ES cells in the presence of 10mM NaBut, digested with trypsin and analyzed by nanoLC-MS as previously published (Waldmann et al., 2011). *S. pombe* histones were acid extracted essentially as described (Pidoux et al., 2004) but extracted in 0.4M HCl rather than 0.4M sulphuric acid. The acid extract containing the histones was dialyzed in SAU150 (7M urea, 20mM sodium acetate pH 5.2, 150mM NaCl, 1mM EDTA pH 8.0, 5μM beta-mercaptoethanol), bound to SP-sepharose (Sigma) and eluted with SAU600 (same as SAU150 but with 600mM NaCl) in a gravity flow column (Biorad). Histone-containing fractions were dialyzed in buffer A (0.1% TFA), loaded on a Vydac 208MS C8 column for RP-HPLC and eluted using the following gradient: 36% buffer B to 62% buffer B within 15.9 ml (53 min), 62% buffer to 90% buffer B in 0.6 ml (2 min) and 90% buffer B to 100% buffer B in 0.7 ml (2.3 min). Fractions were analyzed by SDS-PAGE, the H3 band excised and in-gel digested with trypsin as described (Waldmann et al., 2011). Recombinant H3 from the in vitro HAT assay on octamers and chromatin (Figure S5G) was in-gel digested with 250 or 500ng ArgC (Roche, Germany) as described above.

STAGE tip assisted sample purification of digested samples was achieved essentially as described (Rappsilber et al., 2007). Desalted samples were subsequently analyzed using nanoflow (Agilent 1200 nanoLC, Germany) LC-MS/MS on a linear ion trap (LIT)-Orbitrap (LTQ-Orbitrap XL) mass spectrometer (ThermoFisher, Germany). Peptides were eluted with a linear gradient of 10–60% buffer B (80% ACN and 0.5% acetic acid) at a flow rate of 250 nl/min over 40 or 60min depending on the experiment. Data were acquired using a data-dependent "top 5" method, dynamically choosing the five most abundant precursor ions from

the survey scan (mass range 250−1650Th) in order to isolate and fragment them in the LTQ. All data were acquired in the profile mode and dynamic exclusion was defined by a list size of 500 features and exclusion duration of 30 s with a MMD of 10ppm. Early expiration was disabled to decrease the re-sequencing of isotope clusters. The isolation window for the precursor ion selection was set to 2.0Th. Precursor ion charge state screening was enabled and all unassigned charge states as well as singularly charged ions were rejected. For the survey scan a target value of 1,000,000 (1000 ms maximal injection time) and a resolution of 60,000 at *m/z* 400 were set (with lock mass option enabled for the 445.120024 ion), whereas the target value for the fragment ion spectra was limited to 10,000 ions (200ms maximal injection time). The general mass spectrometric conditions were: spray voltage, 2.3 kV; no sheath and auxiliary gas flow; ion transfer tube temperature, 150°C; collision gas pressure, 1.3 mTorr; normalized collision energy using wide-band activation mode; 35% for MS^2. Ion selection thresholds were 500 or 1000 counts for MS^2 depending on the experiment. An activation q = 0.25 and activation time of 30ms was applied.

MS data were processed into peak lists by DTASuperCharge 2.0b1 (part of the MSQuant 2.0b7 software environment [Mortensen et al., 2010]) and searched with Mascot 2.2 against the human International Protein Index protein database (IPI, version 3.65) combined with frequently observed contaminants and concatenated with the reversed versions of all sequences. The MMD for monoisotopic precursor ions and MS/MS peaks were restricted to 5ppm and 0.8-Da, respectively. For MCF-7, mouse ES and *S. pombe* histone samples the enzyme specificity was set to trypsin (with a maximum of two missed cleavages) allowing cleavage N-terminal to proline and C-terminal to aspartate. Modifications were cysteine carbamidomethylation (fixed) as well as protein lysine acetylation, lysine butyrylation, lysine propionylation, lysine and arginine methylation (all states), lysine formylation, serine/threonine/tyrosine phosphorylation, deamidation (asparagine and glutamine) and methionine oxidation (variable). Protein and peptide identifications were further analyzed and manually verified by inspection of chromatograms and spectra (see Figures S1A and S6B).

For recombinant histones the enzyme specificity was set to ArgC with a maximum of 2 missed cleavages. Modifications were protein lysine acetylation, deamidation (asparagine and glutamine) and methionine oxidation (variable). Protein and peptide identifications were further analyzed and manually verified by inspection of chromatograms and spectra. XIC values of peptide VTIMPKDIQLAR (positions 118-129) and RKSTGGKAPRK (positions 10-18) considering all detected modification states were extracted employing the Xcalibur QualBrowser software and used to calculate combined XIC values for the acetylated and unacetylated peptides, respectively.

Digestion of Chromatin by Micrococcal Nuclease

For a typical experiment, 3-6*10ª7 MCF-7 cells were harvested, washed in PBS, resuspended in cold buffer I (300mM sucrose, 60mM KCl, 15mM NaCl, 5mM MgCl, 0.1mM EDTA pH 8.0, 15mM Tris pH 7.5, 1x protease inhibitors (Roche), 10mM sodium butyrate, 1mM DTT) at a density of 1.5x10ª7 cells/ml. Cell suspension was mixed under gentle vortexing with the same volume of cold buffer II (as buffer I but with 0.5% NP-40) and incubated on ice for 10min to lyse the cell membrane. 8ml of a 40% sucrose cushion was prepared (buffer III: 1.2M sucrose, 60mM KCl, 15mM NaCl, 5mM MgCl, 0.1mM EDTA pH 8.0, 15mM Tris pH 7.5, 1x protease inhibitors, 10mM sodium butyrate, 1mM DTT) and a maximum of 3*10ª7 cells were loaded onto one cushion. The released nuclei were separated from the cyctoplasm by centrifugation at 10,000rpm for 20min in a HB4 swing bucket rotor (Beckman) at 4°C. The nuclei were resuspended in Mnase digestion buffer (320mM sucrose, 4mM MgCl2, 1mM CaCl2, 50mM Tris pH 7.5, 1x protease inhibitors, 10mM sodium butyrate) containing 30U Mnase/ml (Fermentas) at a concentration of 4x10ª7 nuclei/ml. The chromatin was digested for up to 15min at 37°C and digestion was stopped by the addition of 10mM EDTA final concentration. After 15min on ice the digestions were centrifuged at 10.000rpm for 10min and the supernatant saved as "S1" fraction. The pellet was resuspended in dialysis buffer (0.2mM EDTA pH 8.0, 1mM Tris pH 7.5, 1x protease inhibitors, 10mM sodium butyrate) and incubated on the rolling wheel for at least 2h. The samples were centrifuged again and the supernatant "S2" kept. The concentration of chromatin was determined at OD 260nm and digestion of chromatin was monitored by separating 500ng of chromatin on a 1.3% agarose gel after RNase digestion and the addition of 1% SDS final concentration.

Sucrose Gradient Centrifugation of Mnase-Digested Chromatin

5ml of linear sucrose gradients ranging from either 5%–30%, 10%–30% or 10%–40% sucrose in sucrose gradient buffer (50mM HEPES pH 7.5, 50mM KCl, 1mM EDTA pH 8.0, sucrose 5%–40% w/vol, 1x protease inhibitor, 5mM sodium butyrate) were prepared using a Gradient Master (Biocomp). The gradients were overlaid with a maximum of 400μl Mnase-digested chromatin and centrifuged in SW55Ti rotor (Beckman) at 48,000rpm at 4°C for 2.5h–3h in an Optima ultracentrifuge (Beckman). The gradient was fractionated in 150–350μl aliquots. 5μl aliquots of each fraction were RNase-digested at 37°C in 1% SDS for 1h, incubated at 60°C for 10min and analyzed by electrophoresis in a 1% agarose gel in 0.5x TBE.

Immunoprecipitation of Mononucleosomes

The protocol was adapted from Ruthenburg et al. (2011). All fractions of the sucrose gradient that contained mononucleosomes (~150–190bp) were pooled and dialyzed against DB50 buffer (50 mM HEPES pH 7.5, 50 mM KCl, and 1mM EDTA) at 4°C O/N. The dialyzed mononucleosomal fractions were concentrated in an ultrafiltration device (VivaSpin 500, MWCO 30k) by centrifugation aiming at a concentration of ~200ng/μl as determined by OD 260nm. For immunoprecipitation 30μg of mononucleosomes were mixed with 2μg of H3K122ac- or rabbit IgG antibody prebound to 40μl magnetic protein A beads (Thermo) in a final volume of 500μl DB50 buffer supplemented with 5% glycerol, 0.1% NP-40, 50μg/ml BSA, protease inhibitors and 0,5μg/ml TSA. After O/N

IP the beads were washed 3x with DB200 (5% glycerol, 25mM HEPES pH 7.5, 200mM KCl, 0.1% NP-40 and 1mM EDTA) and 2x in 250mM LiCl washing buffer (5% glycerol, 25mM HEPES pH 7.5, 250 mM LiCl, 1mM EDTA, 0.5% sodium deoxycholate and 0.5% NP-40). Beads from three IPs were pooled and bound proteins eluted by boiling in 60μl 2x SDS-loading buffer at 95°C for 10min.

Chromatin Immunoprecipitation of Crosslinked Mononucleosomes

MCF-7 cell nuclei (isolated as described above) were resuspendend in Mnase digestion buffer (320mM sucrose, 4mM $MgCl_2$, 1mM $CaCl_2$, 50mM Tris pH 7.5, 0.2mM AEBSF, 10mM sodium butyrate) with 0.2% formaldehyde and crosslinked at RT for 5min under constant agitation. The fixation was quenched by adding glycine to a final concentration of 25mM for 5min on a rolling wheel. Crosslinked nuclei were washed with Mnase digestion buffer once, pelleted again and resuspendend in Mnase digestion buffer with 60U/ml Mnase (Fermentas) and digested to > 90% mononucleosomes at 37°C for 15min. Digestion was stopped by addition of 10mM EDTA final concentration and transferred to ice. After 15min on ice the samples were centrifuged at 10,000rpm for 10min and the supernatant containing the nucleosomes saved. 80μg of nucleosomes were diluted 1:10 in incubation buffer (50mM Tris pH 7.5, 75mM NaCl, 5mM EDTA pH 8.0, 0.1% NP40, 1x protease inhibitor, 10mM NaBut) and centrifuged at 13.000 rpm for 10min to remove any precipitant. Soluble nucleosomes were incubated with different antibodies prebound to Dynabeads protein A (Invitrogen) at 4°C O/N. The immunocomplexes were collected in a magnetic rack and washed 1x in low salt buffer (50mM Tris pH 7.5, 150mM NaCl, 5mM EDTA pH 8.0, 1% Triton X-100, 0.5% NP-40) and 5x in high salt buffer (50mM Tris pH 7.5, 450mM NaCl, 5mM EDTA pH 8.0, 1% Triton X-100, 0.5% NP-40). After a final wash in TE Buffer, the beads were resuspended in 1,1x elution buffer (110 mM NaHCO3, 1.1% SDS), and the immunocomplexes were eluted in a thermoshaker at 30°C for 30 min. The eluted samples were decrosslinked for at least 5 hr at 65°C in the presence of 20 μg proteinase K (Roche) and subjected to an RNAse digestion with 1 μl of RNase (Roche) at 37°C for 1 hr. DNA was purified with the Qiaquick PCR purification Kit (QIAGEN) according to the manufacturer's instructions and eluted in 80 μl TE buffer. 2μl of eluted ChIP DNA was used for qPCR with a 7300 Real-Time PCR system (Applied Biosystems), the primer sequences are listed in Table S2. For Illumina sequencing the DNA from three individual immunoprecipitations was pooled.

Crosslinked ChIP

MCF-7 cells were grown in 145 mm2 dishes to 80%–90% confluency and fixed by adding formaldehyde (Sigma) to 1% final concentration for 10min at RT, or for the ChIP time course experiment with 1.5% formaldehyde for 5min at 37°C. Fixation was quenched by addition of 125mM glycine final concentration. The cells were washed twice with ice cold PBS and collected by scraping in PBS supplemented with 1x protease inhibitors and 10mM NaBut. Cells were pelleted and resuspendend in 1.2ml RIPA lysis buffer (50mM Tris-HCl pH 8.0, 150mM NaCl, 2mM EDTA pH 8.0, 0.1% SDS, 1% NP-40 (Roche) 0.5% sodium deoxycholate, 1x protease inhibitors and 10mM NaBut) for 1.5*10ª7 cells and incubated on ice for 10min. The lysates were sonicated with a Bioruptor (Diagenode) to an average size of ~300–800 bp or ~200bp for ChIP time course experiment. The sonicated samples were centrifuged at 17,000 g for 10min and the supernatant, containing the soluble chromatin, was flash- frozen in liquid N_2 and stored at −80°C after taking 50μl of chromatin as input to determine the concentration of chromatin. The 50μl input material was mixed with 127μl 1.6x elution buffer (160mM $NaHCO_3$, 1.6% SDS), supplemented with 1μl RNase (Roche) and incubated at 37°C for 1h. Next, 20μg proteinase K (Roche) and 20μl of 5M NaCl were added and incubated at 65°C for at least 5h to reverse the crosslinking. DNA was purified with the Qiaquick PCR purification Kit (QIAGEN) and eluted in 100μl. For immunoprecipitation with H3K122ac antibody an equivalent to 25μg DNA was used, for estrogen receptor ChIP an equivalent to 250μg DNA was used. Prior to immunoprecipitation the chromatin was diluted 1:5 with dilution buffer (20mM Tris pH 8.0, 150mM NaCl, 2mM EDTA pH 8.0, 1% Triton X-100, 1x protease inhibitors and 10mM NaBut) and precleared with 20μl washed protein A sepharose beads (Amersham), 1.5μg sonciated salmon sperm DNA (Sigma) and 4μg BSA (NEB) per IP. The precleared chromatin was incubated with different antibodies overnight at 4°C as indicated. Next day 20μl of 50% protein A slurry blocked with sonicated salmon sperm DNA and BSA was added to collect the immunocomplexes for 2h at 4°C. The bound immunocomplexes were washed once with dilution buffer and five times with LiCl buffer (500mM LiCl, 50mM HEPES, pH 8.0, 1mM EDTA pH 8.0, 1% NP-40, 0.7% sodium deoxycholate) for 10min. After a final wash in TE buffer the beads were resuspended in 180μl freshly prepared 1.1x elution buffer (110mM NaHCO3, 1.1% SDS) and the immunocomplexes eluted by incubation at 30°C. The eluates were de-crosslinked and purified as described for the input (see above). 2μl of eluted ChIP DNA were used for qPCR, primers are listed in Table S2. For the p300 ChIP-seq experiment 500μg of chromatin were used and the immunocomplex collected with BSA-blocked protein A magnetic beads instead of protein A sepharose beads, primers for validation are listed in Table S3.

Histone Acetyltransferase Assay

The histone substrates were mixed in a final reaction volume of 30μl in 1x histone acetyltransferase (HAT) buffer (5% glycerol, 50mM NaCl, 50mM Tris pH 8.0, 0.1mM EDTA, 10mM sodium butyrate, 1x protease inhibitor, 1mM DTT). Ac-CoA (Sigma) was added to 30μM (for radioactive assays AcCoA was mixed 1:1 with and ^{3}H-Ac-CoA (Perkin Elmer)) and different sources of enzymes were used as indicated in the figure legends and incubated at 30°C for 1h. For the inhibition of p300/CBP HAT activity, 50μM of C646 (Chembiochem) were added to the reaction. The reaction was stopped by adding 10μl of 4xSDS-loading buffer and boiling for

5 min at 95°C. Aliquots were subjected to SDS-PAGE, transferred to nitrocellulose membranes and subjected to autoradiography and immunoblotting.

Recombinant Histone Purification

Recombinant histones with and without acetylation were expressed in BL21(DE3)pLysS as described by (Neumann et al., 2009). Histone purification was carried out as described by (Luger et al., 1999) with slight modifications: For purification of acetylated histones 20mM nicotinamide was added to all nondenaturating buffers. Briefly, inclusion bodies from 1L bacterial culture were solubilised in 20 ml unfolding buffer (7M guanidium hydrochloride, 20 mM Tris pH 7.5, 10 mM DTT) for 1h at RT. After centrifugation the supernatant was dialyzed at 4°C against three changes of 2L freshly prepared SAU200 buffer (7M urea, 20mM sodium acetate pH5.2, 200mM NaCl, 1mM EDTA pH 8.0, 5mM beta-mercaptoethanol). Next the cleared supernatant was loaded on a 6ml ResourceS cation exchange column (GE Healthcare) equilibrated with SAU200 buffer and separated with a ÄKTA Prime HPLC (GE Healthcare) in 40ml of a linear gradient from 0%–100% of SAU200 (A) to SAU600 (B). For H4 the gradient was changed to 30%–100% B. Fractions were analyzed by SDS-PAGE and those containing pure histones were pooled and dialyzed against three changes of 2L dH_2O supplemented with 2mM beta-mercaptoethanol. Dialyzed, soluble histones were lyophilized in aliquots of 1-2mg and stored at −80°C. ResourceS-purified H3K122ac still contained truncated H3 polypeptide from residue 1–121. Full length H3K122ac was successfully separated from truncated H3 1-121 polypeptide by octamer reconstitution and subsequent gel filtration.

Octamer Reconstitution

Histone octamers were refolded from the four individual core histones following a protocol described by (Luger et al., 1999). Briefly, the lyophilized histones were resuspended in unfolding buffer at a concentration of 1μg/μl and incubated at RT for 1h. Equimolar amounts of the four core histones were mixed for another 30min and dialyzed against three changes of 2L refolding buffer (10mM Tris pH 7.5, 1mM EDTA pH 8.0, 2M NaCl, 5mM B-mercaptoethanol) at 4°C O/N. Precipitated material was removed by centrifugation and the supernatant concentrated to 300–400μl in VivaSpin 4 ultrafiltration devices. Refolded octamers were separated from aggregates, tetramers and dimers by gel filtration through a Superdex200 HR 10/30 column connected to a ÄktaExplorer HPLC system (GE Healthcare). Fractions of 400μl were collected and analyzed for histone content and stoichiometry by SDS-PAGE. Fractions containing stoichiometic amounts of all four histone were pooled, concentrated to 2μg/μl in VivaSpin 500 ultrafiltration devices, supplemented with 50% glycerol final concentration and stored at −20°C.

Chromatin Assembly by NAP1 and ACF

Chromatin was assembled onto the pG5-MLP plasmid in vitro with the histone chaperone NAP1 and chromatin remodeling complex ACF (Ito et al., 1997). ACF complex was kindly provided by Gernot Längst. 1μg chromatin assembly reactions were carried out in siliconized reaction tubes in 140μl final volume HEG buffer (25mM HEPES pH7.6, 0,1mM EDTA, 10% glycerol) supplemented with 0.2mM AEBSF, 2mM NaBut, 1mM DTT and 100ngr/μl BSA (NEB). 1M KCl was added to a final concentration of 50mM, taking into account any salt from proteins. Histone octamers were diluted in HEG buffer to 100ng/μl and different amounts added to the buffer. Next dNAP1 (4.8μg diluted in 2μl HEG buffer) was added to the reaction, which was mixed and incubated at RT for 30min. ATP-regenerating system (ATP-mix) was prepared by mixing 49.5μl HEG buffer, 90μl 500mM of creatine phosphate, 1.5μl of creatine phosphokinase (5μg/μl), 9μl of 500mM ATP and 30μl 250mM $MgCl_2$. After 30min the following components were added subsequently and immediately mixed by gentle vortexing: 2μl of ACF (70ng/μl in HEG buffer), 16.8μl ATP mix, 10μl of plasmid DNA (100ng/μl in HEG buffer). The reaction was spun down gently and incubated at 27°C for 210min. The efficiency of the reaction was tested by micrococcal nuclease digestion of 500ng chromatin with 25 or 125mU Mnase (Fermentas) at 2mM $CaCl_2$ at 30°C for 10min and topoisomerase I relaxation of 200ng chromatin (or naked DNA) with 10U *Vaccinia* topoisomerase I (Epicenter) at 2.5mM $MgCl_2$ at 37°C for 30min. The DNA was isolated by phenol-chloroform extraction, ethanol-precipitated and analyzed by 1.3% or 1% agarose gel electrophoresis in 0.5% TBE and subsequent staining with ethidium bromide.

In Vitro Transcription

In vitro transcription (IVT) was performed as previously described (Margueron et al., 2008) with a few modifications. Briefly, for one transcription reaction 20–50ng of chromatin purified by sucrose gradient centrifugation or naked DNA (pG5-MLP, kindly provided by Guohong Li) in 7μl TE were mixed with 6μl BC100. 1μl of GAL4-VP16 (20–40ng/μl) activator were added and incubated at RT for 15min to allow binding to the GAL4 binding sites on pG5-MLP. Next 7.2μl C-mix (55mM HEPES-KOH pH 7.9, 22mM MgCl2, 8.5% (w/v) PEG8000, BSA 425ng/μl, 17mM DTT, 160mM AmSO4), 1μl coactivator p300 (30-60ng/μl) and 1μl of an AcCoA/NaBut mix (500μM Ac-CoA/200mM NaBut /0.3μl BC100) were added and incubated at 30°C for 30min. Next 10μl HeLa nuclear extract (prepared according to Dignam et al. [1983]) were added to the reaction and incubated at 30°C for 30min. Transcription was started by the addition of 3μl of a rNTP-mix with limiting amounts of radioactive rUTP (16.5μl of 12mM rATP, rGTP and rCTP, 5.5μl rUTP 32P (Perkin BLU007H), 4.4μl RNAsin (Promega), 6.6μl ddH2O) and carried out at 30°C for 20min. The transcription was chased by adding 6μl rUTP-mix (600μM cold rUTP, 6U/μl Rnase T1) at 30°C for another 20min. Transcription and T1 Rnase digestion were stopped with 150μl stop buffer (20mM EDTA, 1% SDS). The RNA was phenol/chloroform extracted and ethanol precipitated in the presence of glycogen (Invitrogen). The dried pellet was resuspended in 15μl RNA loading buffer (Formamide/Tris/EDTA/Xylene/Cyanol/Bromophenol Blue), incubated at 95°C for 5min and separated by electrophoresis through an urea denaturating polyacrylamid gel

(urea 4.2g, 10x TBE 1ml, 40% acrylamide (30:0.8) 1.6ml, 10% APS 100ul, TEMED 10μl, 10ml final volume) in 1xTBE at 150V for 1h. The gel was vacuum-dried on a Whatman paper and the radioactivity detected with a storage phosphor screen (GE Healthcare) imaged in a Typhoon 9200 scanner (GE Healthcare).

In Vitro ChIP

For in vitro ChIP chromatin was prepared and processed exactly as described for in vitro transcription until the addition of HeLa nuclear extract (preinitiation complex formation, see protocol for in vitro transcription and also Figure 3A). 30min after addition of 10μl HeLa nuclear extract (with 100ng/μl pSL plasmid DNA) at 30°C chromatin was crosslinked by the addition of formaldehyde to 1% final concentration at 30°C for 5min and quenched with 125mM glycine final concentration. Crosslinked chromatin was adjusted to 1% SDS and sonicated with a Bioruptor (Diagenode) two times for 10min (settings ''high'' and 30 s on/off cycle). Soluble chromatin was diluted tenfold with dilution buffer (20mM Tris pH 8.0, 150mM NaCl, 2mM EDTA pH 8.0, 1% Triton X-100, 1x protease inhibitors) and precleared as described for crosslinked ChIP above. Immunoprecipitation, purification of DNA and qPCR analysis were performed exactly as described for crosslinked ChIP, primers for pG5-MLP promoter were: pG5MLPFor ACTCCGACTCTAG AGGATCCC, pG5MLPRev GGGAAGAGAGTGAGGACGAAC.

Histone Eviction Assay

The histone eviction assay was adapted from a protocol developed for histone eviction from the HTLV promoter (Sharma and Nyborg, 2008). The pG5-MLP promoter template of ~620bps was amplified and end labeled with biotin (5') by PCR, Forward primer (biotinylated) ATAACCTTATGTATCATACACAT, reverse primer GCCTAGGGGAGTGGAATGA (MWG Eurofins). Chromatin was assembled by step-wise salt dialysis (Figure S3F) and immobilized with Dynabeads M-280 streptavidin (Invitrogen) in chromatin binding buffer (20 mM HEPES at pH 8.0, 150 mM KCl, 10% glycerol, 4 mM MgCl2, 1 mM DTT, 200ng/μl BSA, 5mM Nabut) at 4°C for 3h, washed and stored in immobilized template binding buffer (ITBB) (120 mM KCl, 10 mM HEPES at pH 8.0, 5% glycerol, 200 ng/μL BSA, 0.05% NP-40, 5mM NaBut). For the eviction assay 500μg immobilized chromatin was incubated with 500μg GAL4-VP16 in ITBB for 15min at 30°C. Next 1μg p300, 2.5μg NAP1, 1μg supercoiled pSL acceptor DNA and AcCoA (30mM final) were added and incubated at 30°C as indicated. After the reaction the magnetic beads were collected and the supernatant (evicted fraction) saved. The beads were washed twice in ITBB, eluted in SDS sample buffer and analyzed together with the evicted fraction by SDS-PAGE and immunoblot.

Sequencing and Data Analysis

Processing of ChIP-Seq Libraries

ChIP-seq libraries were sequenced on the Illumina GA-II platform and the raw images processed using the Solexa pipeline. All libraries were aligned to the human genome (built hg18). The H3K122ac, H3K27ac, H2A.Z and H2A.Zac input ChIP-seq libraries were prepared and processed by the in-house sequencing facility at the Max Planck Institute for Immunobiology and Epigenetics and aligned using Bowtie 2 (Langmead and Salzberg, 2012) with default settings, the *p300* and matched input libraries were prepared and processed by the sequencing facility of the Genome Institute of Singapore and were aligned with ELAND (Illumina). To avoid potential artifacts caused by PCR amplification, reads mapping to the exact genome coordinates were considered as one. Table S4 lists details of ChIP-seq, DNaseI-seq and Gro-seq libraries that have been used in our analyses, including those available from public sources.

Peak Calls and Genomic Regions Used in This Study

Regions enriched for H3K122ac were obtained using the peak calling software CCAT3.0 (Xu et al., 2010). CCAT was run in 'region' mode with default parameters except for read length, which was set to the empirically determined fragment length of 170bps. Regions below an FDR of 1% were retained for further analysis. Similarly, p300 peaks were obtained with CCAT using default settings in 'peak' mode. To characterize the distribution of H3K122ac in detail we used several additional sets of 'genomic landmarks'. Transcription start sites (TSS) of coding and non-coding regions were obtained from RefGenes and Gencode tables downloaded from the UCSC genome browser (http://genome.ucsc.edu/; genome built hg18). DNaseI hypersensitive regions and peak calls for several transcription factors were obtained from publicly available sources. Peak data from the ENCODE project were obtained on hg19 and lifted to hg18 using liftOver (ratio set to 0.95) (Kent et al., 2002) prior to any analysis. A list of all ChIP-seq and DNaseI-seq peak regions used in this study is listed in Table S5. In addition, for several analyses we used a set of MCF-7 enhancer regions. To be able compare H3K122ac to H3K4me1 and H3K27ac at enhancers in an unbiased fashion, we used an enhancer definition that was independent of these histone marks. We defined enhancers as regions of 500bps centered on the middle of DHS that were located > 2.5kb away from TSS annotated in the RefGene table. Furthermore we also required a minimum of 25 sequencing reads from the p300 ChIP-seq library. This approach yielded a total of 2883 enhancer regions.

Bedtools

Analyses based on comparing and processing genomic interval data were performed using BEDtools v2.16.2 (Quinlan and Hall, 2010). Overlaps between genomic intervals were determined using *intersect* with –u and –v option to obtain shared or unique regions, respectively. *Shuffle* was used to create sets of randomized genomic regions that match the size distribution of the given input regions. The option –chrom was used to maintain the same frequency of sites across chromosomes as compared to the input. To

annotate intervals with interval-based features and to obtain counts of sequencing reads covering the intervals *annotate* was used with the option -counts. To obtain distribution of read counts across larger regions, intervals were first split into 10bp windows using *makewindows*. Number of sequencing reads falling onto each window was then determined using *coverage*. To display sequencing data bedGraph files were prepared from BED files of aligned sequencing reads using *genomecoverage* with the –bg option. Libraries were scaled to 10M reads (-scale) and displayed on UCSC genome browser (http://genome.ucsc.edu) (Kent et al., 2002).

Statistical Analyses

If not further specified statistical analyses and plotting of data were performed using the appropriate core functions in R. The pairwise correlation between ChIP-seq libraries at specific loci (TSS or DHS) were calculated by correlating the normalized tag counts between two marks.

Aggregation Plots

In addition to bedtools coverage, the Agg.py script from the ACT package (Jee et al., 2011) was used to obtain average counts of sequencing reads around genomic landmarks (TSS and TFBS). Average read densities were displayed as line graphs using R.

Gene Expression and Transcriptional Activity at DHS

Gro-seq data from Hah et al. (2011) were used to 1) group RefGenes according to their expression levels into quartiles and 2) compare transcriptional activity between DHS with high and low levels of H3K122ac. To assess transcriptional activity at H3K122ac marked DHS we compared the number of Gro-seq reads at DHS with high H3K122ac read count (top 10%) and the rest of DHS. In addition, we assessed whether transcription originated at these sites. Reads mapping to forward and reverse strand were separated and average read count was obtained for 10bp windows throughout a 2kb region centered in the middle of the DHS. Distribution of Gro-seq reads on forward and reverse strand clearly suggested transcriptional initiation at DHS sites with high H3K122ac levels.

Peak Annotation

The ChIP-seq analysis software Homer (Heinz et al., 2010), and more specifically, annotatePeak.pl was used to obtain the distance from each H3K122ac peak region to the closest coding transcript.

S. pombe Strains and Culture, nmt1+ Induction, and Gene Expression Analysis

S. pombe strains are listed in Table S6. For *nmt1+* gene activation experiments, pre-cultures were grown for 24h in PMG + 1 μg/ml thiamine. The same number of cells was added to the main cultures (medium A and B) in order to reach a target OD (600nm) of 0.5 (exponential growth) 12 hr later. Medium A *nmt1+* repressed: 50 ml culture of PMG + 1 μg/ml Thiamine; Medium B *nmt1+* induced: 50 ml culture of PMG without thiamine. Expression of the *nmt1+* gene in the induced condition (B) was quantified relative to the culture growing in parallel under repressed conditions (A). A 10 ml aliquot was removed at 13, 14, 15 and 22 hr after induction for RNA isolation. RNA isolation, cDNA synthesis and qRT-PCR were performed as described (Emmerth et al., 2010), except that quantitative RT-PCR was performed on a Bio-Rad CFX96™ Real-Time PCR System. Primers are listed in Table S1.

SUPPLEMENTAL REFERENCES

Dignam, J.D., Lebovitz, R.M., and Roeder, R.G. (1983). Accurate transcription initiation by RNA polymerase II in a soluble extract from isolated mammalian nuclei. Nucleic Acids Res. *11*, 1475–1489.

Ekwall, K., Cranston, G., and Allshire, R.C. (1999). Fission yeast mutants that alleviate transcriptional silencing in centromeric flanking repeats and disrupt chromosome segregation. Genetics *153*, 1153–1169.

Emmerth, S., Schober, H., Gaidatzis, D., Roloff, T., Jacobeit, K., and Bühler, M. (2010). Nuclear retention of fission yeast dicer is a prerequisite for RNAi-mediated heterochromatin assembly. Dev. Cell *18*, 102–113.

ENCODE Project Consortium. (2011). A user's guide to the encyclopedia of DNA elements (ENCODE). PLoS Biol. *9*, e1001046.

Freeman, L., Kurumizaka, H., and Wolffe, A.P. (1996). Functional domains for assembly of histones H3 and H4 into the chromatin of *Xenopus* embryos. Proc. Natl. Acad. Sci. USA *93*, 12780–12785.

Hah, N., Danko, C.G., Core, L., Waterfall, J.J., Siepel, A., Lis, J.T., and Kraus, W.L. (2011). A rapid, extensive, and transient transcriptional response to estrogen signaling in breast cancer cells. Cell *145*, 622–634.

He, H.H., Meyer, C.A., Shin, H., Bailey, S.T., Wei, G., Wang, Q., Zhang, Y., Xu, K., Ni, M., Lupien, M., et al. (2010). Nucleosome dynamics define transcriptional enhancers. Nat. Genet. *42*, 1–6.

Heinz, S., Benner, C., Spann, N., Bertolino, E., Lin, Y.C., Laslo, P., Cheng, J.X., Murre, C., Singh, H., and Glass, C.K. (2010). Simple combinations of lineage-determining transcription factors prime cis-regulatory elements required for macrophage and B cell identities. Mol. Cell *38*, 576–589.

Jee, J., Rozowsky, J., Yip, K.Y., Lochovsky, L., Bjornson, R., Zhong, G., Zhang, Z., Fu, Y., Wang, J., Weng, Z., and Gerstein, M. (2011). ACT: aggregation and correlation toolbox for analyses of genome tracks. Bioinformatics *27*, 1152–1154.

Joseph, R., Orlov, Y.L., Huss, M., Sun, W., Kong, S.L., Ukil, L., Pan, Y.F., Li, G., Lim, M., Thomsen, J.S., et al. (2010). Integrative model of genomic factors for determining binding site selection by estrogen receptor-α. Mol. Syst. Biol. *6*, 456.

Kent, W.J., Sugnet, C.W., Furey, T.S., Roskin, K.M., Pringle, T.H., Zahler, A.M., and Haussler, D. (2002). The human genome browser at UCSC. Genome Res. *12*, 996–1006.

Mortensen, P., Gouw, J.W., Olsen, J.V., Ong, S.E., Rigbolt, K.T., Bunkenborg, J., Cox, J., Foster, L.J., Heck, A.J., Blagoev, B., et al. (2010). MSQuant, an open source platform for mass spectrometry-based quantitative proteomics. J. Proteome Res. *9*, 393–403.

Pidoux, A., Mellone, B., and Allshire, R. (2004). Analysis of chromatin in fission yeast. Methods *33*, 252–259.

Quinlan, A.R., and Hall, I.M. (2010). BEDTools: a flexible suite of utilities for comparing genomic features. Bioinformatics *26*, 841–842.

Rappsilber, J., Mann, M., and Ishihama, Y. (2007). Protocol for micro-purification, enrichment, pre-fractionation and storage of peptides for proteomics using StageTips. Nat. Protoc. *2*, 1896–1906.

Ross-Innes, C.S., Stark, R., Teschendorff, A.E., Holmes, K.A., Ali, H.R., Dunning, M.J., Brown, G.D., Gojis, O., Ellis, I.O., Green, A.R., et al. (2012). Differential oestrogen receptor binding is associated with clinical outcome in breast cancer. Nature *481*, 389–393.

Waldmann, T., Izzo, A., Kamieniarz, K., Richter, F., Vogler, C., Sarg, B., Lindner, H., Young, N.L., Mittler, G., Garcia, B.A., and Schneider, R. (2011). Methylation of H2AR29 is a novel repressive PRMT6 target. Epigenetics Chromatin *4*, 11.

Xu, H., Handoko, L., Wei, X., Ye, C., Sheng, J., Wei, C.L., Lin, F., and Sung, W.K. (2010). A signal-noise model for significance analysis of ChIP-seq with negative control. Bioinformatics *26*, 1199–1204.

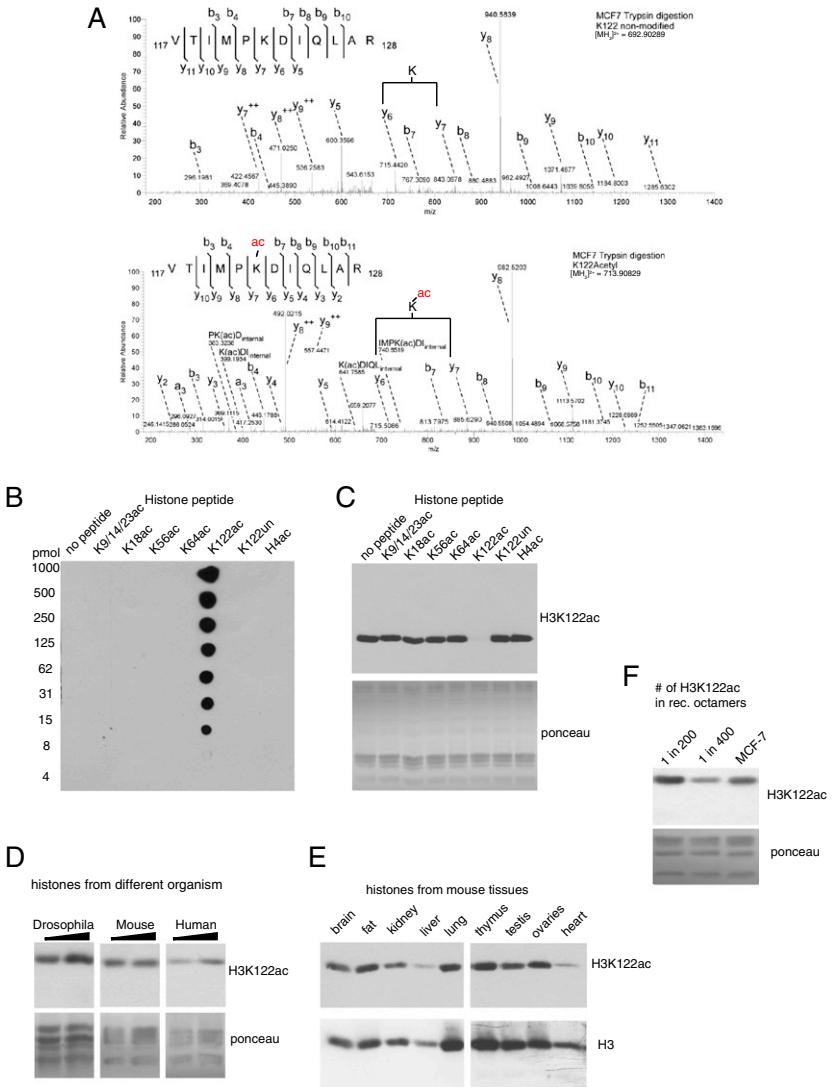

Figure S1. Detection of H3K122ac in MCF-7 Cells by Mass Spectrometry and in Different Organisms by Immunoblotting, Related to Figure 1

(A) CID tandem MS spectra of the tryptic histone H3 peptide VTIMPK$_{122}$DIQLAR in both its unmodified and acetylated form, the m/z values of the peptides are shown in the upper right corner. The top spectrum shows the unmodified, the bottom spectrum the modified peptide with a mass shift of ~42 Da in the ion series between the y6 and the y7 ion, which indicates the presence of an acetyl group at H3K122 (Kac). The assigned b- and y-type ions are depicted in the spectra. The acetyl modification enabled the detection of additional internal fragments covering modified H3K122. The high mass accuracy of ~2ppm allowed unambiguous discrimination of tri-methyl from H3K122 acetyl modification. Virtually identical data were obtained for mouse ES cells (data not shown).

(B) Immunodot blot assay with H3K122ac antibody. Peptides with acetylations at indicated residues within H3, unmodified H3K122 (H3K122un) and tetra-acetylated H4 at K5/8/12/16 (H4ac) were spotted in serial dilutions and detected with the H3K122ac antibody.

(C) Peptide competition experiment with H3K122ac antibody in immunoblot on MCF-7 histones. The H3K122ac-specific antibody was pre-absorbed with 100pmol/ml of the same peptides as in (B). Competition is specific for the H3K122ac peptide.

(D) H3K122 is acetylated in histones from *Drosophila*, mouse and human cell lines. Two amounts of acid extracted histones (as indicated by triangle) from Schneider 2 cells (*Drosophila* m.), embryonic stem cells (mouse) and MCF-7 cells (human) were immunoblotted with antibody against H3K122ac. Ponceau serves as loading control.

(E) H3K122ac is present in multiple mouse tissues. Acid extracted histones from the indicated mouse tissues were immunoblotted with antibodies against H3K122ac and general H3 as a loading control. Note that in general the H3K122ac signal follows the H3 signal.

(F) Approximation to level of H3K122ac in MCF-7 cells. Immunoblot of histones from untreated MCF-7 cells, and a mixture of recombinant H3 wt histone octamers and recombinant H3K122ac octamers (0.25% and 0.125% or 1 in 200 and 1 in 400 nucleosomes with K122ac, respectively). H3K122ac signal in histones from asynchronously growing MCF-7 cells is 80% from 1 in 200 dilution as determined by densitometry (ImageJ). We hence estimate that one in 250 H3 is acetylated at K122. For more details on H3K122ac octamers see also Figures 3 and S3.

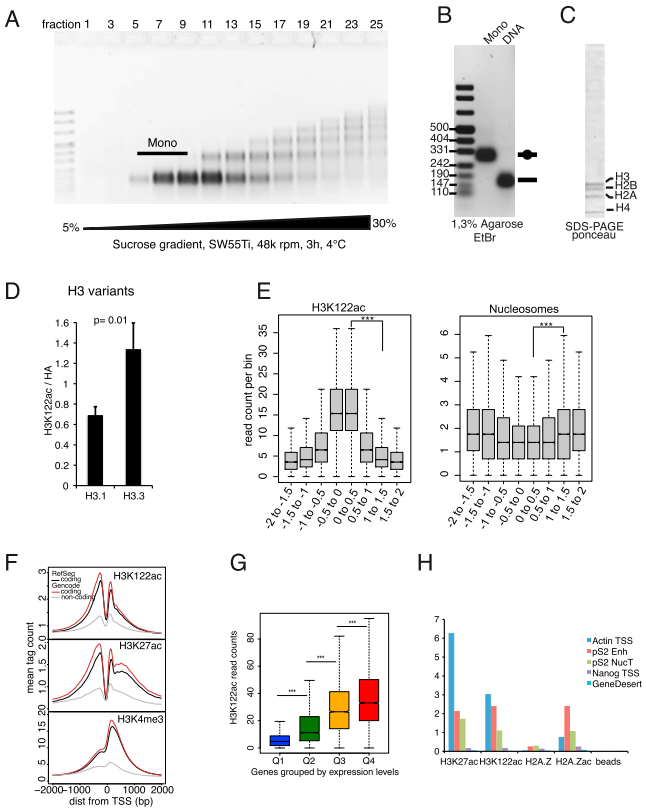

Figure S2. Preparation of Pure Mononucleosomes from MCF-7 Cells and Validation of ChIP-Seq Data, Related to Figure 2

(A) Mononucleosome preparation for H3K122ac immunoprecipitation. Nucleosomes were released by *in nucleo* digestion of MCF-7 chromatin with micrococcal nuclease (adapted from Ruthenburg et al. [2011]). Soluble nucleosomes were subjected to centrifugation in a 5%–30% sucrose gradient and the fractions analyzed by agarose gel electrophoresis and ethidium bromide staining. Fractions 5–9 (labeled "Mono") contained mononucleosomes and were pooled for subsequent immunoprecipitation.

(B) Integrity of pooled mononucleosomes. Mononucleosomes ("Mono") were analyzed by agarose gel electrophoresis and ethidium bromide staining. Naked DNA purified from mononucleosomes was loaded next to the mononucleosomes to mark the size of potentially unwrapped DNA and visualized with ethidium bromide.

(C) Stoichiometry of histones in mononucleosomes. Mononucleosomes were separated by SDS-PAGE, transferred to a nitrocellulose membrane and visualized by ponceau staining. The migration of the four core histones is indicated on the right.

(D) Related to Figure 2B: Bar graph displays the average enrichment of H3K122ac on H3.3 relative to H3.1 and the standard deviation from three independent experiments. Statistical significant difference (p = 0.01) was calculated by two-tailed t test.

(E) Regions enriched in H3K122ac as determined by ChIP-Seq show reduced nucleosome occupancy. Shown are H3K122ac (left) and nucleosome reads (right) in 500bp bins from the center of all H3K122ac peak regions in window -/+ 2kb. There is significant enrichment of H3K122ac ($p < 2.2*10^{-16}$) and depletion of nucleosomes ($p < 2.2*10^{-16}$) when comparing the signal from the peak summit (0–0.5kb) and surrounding regions (1–1.5kb).

(F) H3K122ac at TSS of non-coding genes is comparable to other active histone marks. Aggregation plots show the enrichment of H3K122ac, H3K27ac and H3K4me3 around the TSS of coding and non-coding genes (Gencode annotation). TSSs of coding genes annotated in the RefGene table, which were used throughout this study, were included for comparison. Overall, H3K122ac enrichment at TSS of non-coding genes is markedly lower compared to coding genes. Note that all three marks show similarly low levels of enrichment at non-coding TSSs, suggesting that H3K122ac has no unique function at these TSSs.

(G) H3K122ac enrichment at genes differs significantly between all four quartiles of expression levels. Shown are H3K122ac normalized read counts in a 2kb window with the TSS centered in the middle, outliers were omitted for a better visualization. All p-values were $< 2.2*10^{-16}$.

(H) ChIP-qPCR verifies specific enrichment of H3K122ac, H3K27ac, H2A.Z and H2A.Zac. MCF-7 nucleosomes were immunoprecipitated with the indicated antibodies and the DNA analyzed by qPCR for enrichment at indicated promoters (TSSs), known intergenic enhancers (Enh) or gene-free (GeneDesert) regions relative to input. Primers are listed in Table S2.

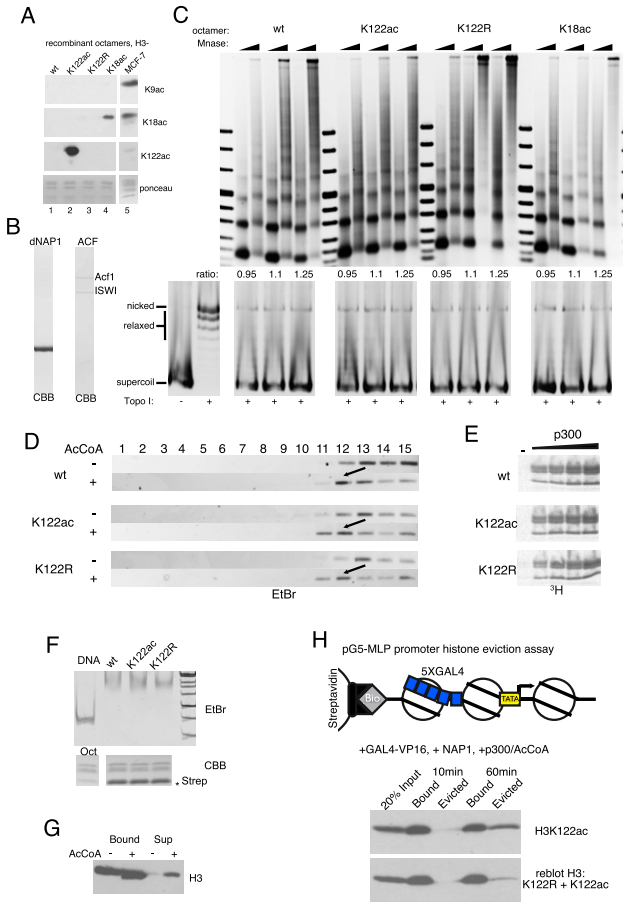

Figure S3. Assembly of Chromatin with Site-Specific Acetylation at H3K122 and Histone Eviction Assay, Related to Figure 3

(A) The site-specific acetylation of histone octamers (lanes 1-4) used in Figure 3B was validated by immunoblot with H3K9ac, H3K18ac and H3K122ac- specific antibodies in comparison to endogenous histone from MCF-7 cells treated with 10mM NaB (lane 5).

(B) dNAP1 histone chaperone and ACF chromatin remodeling complex. The purity of recombinant dNAP1 and Acf1 and ISWI polypeptides of the ACF complex used for chromatin assembly reaction was checked by SDS-PAGE and Coomassie Brilliant Blue (CBB) staining.

(C) Chromatin assembly with histone octamers containing either WT H3 (wt), H3K122ac, H3K122R or H3K18ac. For each octamer three different octamer to DNA (pG5-MLP plasmid) ratios were tested for dNAP1/ACF-mediated chromatin assembly by limited micrococcal nuclease digestion (Mnase, upper panel) and topoisomerase I relaxation (Topo I, bottom panel). Based on this an octamer to DNA ratio was chosen that resulted in a ladder of well-positioned nucleosomes and supercoiled plasmid DNA (for wt: 1.15:1, K122ac: 1.15:1, K122R: 0.95:1, K18ac: 1.1:1). Efficient relaxation of naked DNA by topoisomerase is shown in the lower panel on the left. For IVT, chromatin was purified by 10%–40% sucrose gradient centrifugation and only the peak fractions were used (same fractions for all four chromatin preparations, data not shown).

(D) H3K122ac does not change chromatin compaction in a detectable manner. Chromatin assembled with wt, H3K122ac or H3K122R octamers was incubated with GAL4-VP16, p300 and -/+ AcCoA for 1h and assayed by 10%–30% (fractions 1–15) sucrose gradient centrifugation for AcCoA-dependent chromatin decompaction. The shift in peak fractions between -/+ AcCoA (agarose gel with EtBr staining) is indicated by a black arrow. A representative experiment is shown.

(E) H3K122ac does not have an impact on global chromatin acetylation by p300. Chromatin assembled with wt, H3K122ac or H3K122R octamers was incubated for a HAT assay with GAL4-VP16 or ^{3}H-AcCoA and increasing amounts of p300 for 30min. ^{3}H incorporation shows comparable chromatin acetylation in all three chromatin preparations.

(F) Chromatin assembly on linear template of pG5-MLP promoter. A linear template of the pG5-MLP promoter (~620bp) was efficiently assembled in chromatin as shown by the shift in migration relative to naked DNA (native PAGE, EtBr staining). The bottom panel shows stoichiometry of histones in chromatin immobilized on magnetic streptavidin beads as visualized by Coomassie Brilliant Blue staining, the asterisk indicates migration of streptavidin.

(G) Linear, immobilized chromatin was incubated with GAL4-VP16, NAP1, p300 and ± AcCoA for a histone eviction assay (see 3F) for 60min. After the reaction the supernatant (Sup) and template-bound fractions (Bound) were assayed for histone H3 by immunoblot. Histone eviction was stimulated by AcCoA as described previously (Ito et al., 2000; Sharma and Nyborg, 2008).

(H) Histone eviction assay demonstrates preferential eviction of H3K122ac over H3K122R from immobilized pG5-MLP promoter template. Chromatin was assembled with a mixture of H3K122R and H3K122ac octamers (ratio 5:1) that cannot be further acetylated at H3K122 at any point during the eviction assay. After 10min and 60min in the presence of GAL4-VP16, NAP1 and p300/AcCoA the supernatant ("evicted") and template-bound fraction were separated and were assayed for global H3 content (H3K122R and H3K122ac) and H3K122ac only by immunoblot with a general H3 and the H3K122ac antibody.

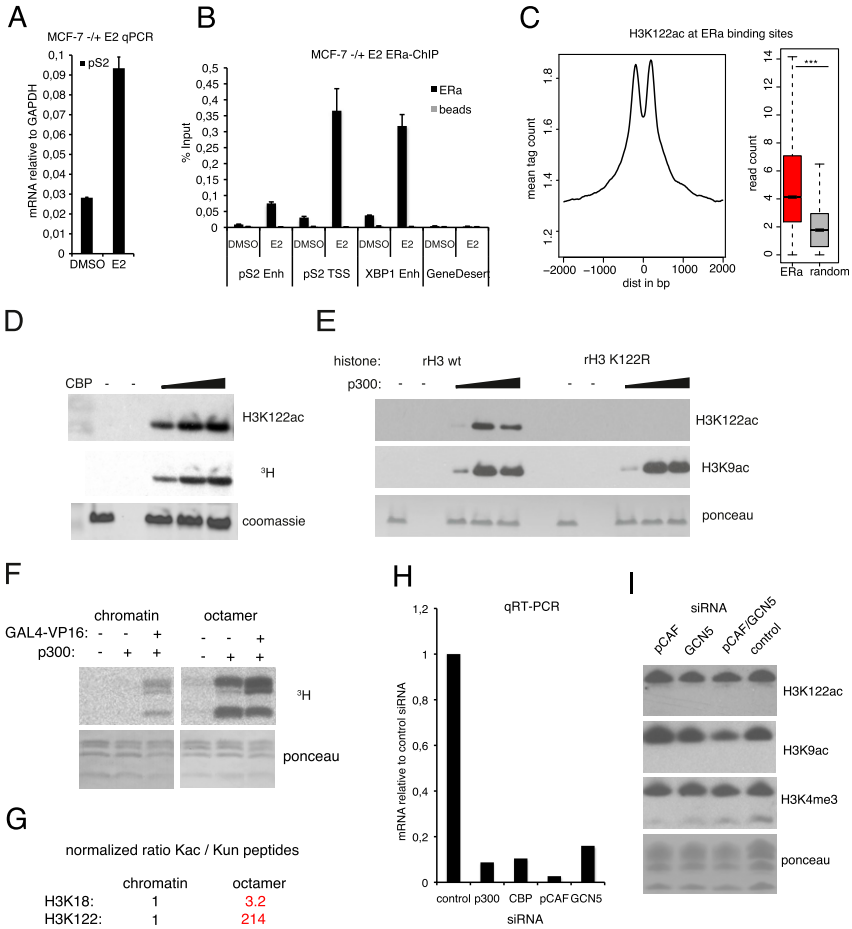

Figure S4. H3K122ac Is Induced by Estrogen Stimulation and Is Catalyzed by p300/CBP, Related to Figure 4

(A) Transcriptional changes in MCF-7 cells induced by estrogen (17β-*estradiol*, "E2") treatment. MCF-7 cells were deprived of hormones for 72h and stimulated with 10nM E2 for 4h. *pS2(TFF1)* was normalized to *GAPDH* transcript and is upregulated ~3.3-fold. Shown are the average and standard deviations from two experiments. Primers are listed in Table S1.

(B) ERα is recruited to known estrogen response elements (EREs) by estrogen treatment. ChIP was performed with ERα antibody or beads and with chromatin from MCF-7 cells that were treated for 45min with estrogen or DMSO (control) prior to fixation. Depicted is the % input recovery and standard deviation from two experiments. Primers are listed in Table S2.

(C) H3K122ac is globally enriched at ERα binding sites. The normalized tag count of H3K122ac is plotted in a window -/+ 1kb from ERα binding sites in MCF-7 cells (Ross-Innes et al., 2012). Statistically significant enrichment of H3K122ac at ERα binding sites relative to random genomic regions is shown in the box plot on the right ($p < 2.2*10^{-16}$).

(D) In vitro HAT assays with recombinant CBP. Recombinant H3 was incubated with recombinant CBP for an in vitro HAT reaction and was immunoblotted with the H3K122ac antibody.

(E) Specificity of H3K122ac antibody in in vitro HAT assays. Recombinant H3 WT (rH3 wt) or the H3K122R mutant (rH3 K122R) were incubated with increasing amounts of recombinant p300 for in vitro HAT reaction and immunoblotted with H3K9ac and H3K122ac antibody. Note that no H3K122ac signal is detected on the H3K122R mutant, but that there is no effect on the H3K9ac signal. Ponceau staining shows equal loading.

(F) Radioactive in vitro HAT assay was performed with p300 and -/+ Gal4-VP16 and either recombinant WT histone octamers alone (right) or octamers assembled onto the pG5-MLP plasmid (left). Global HAT activity is visualized by ^{3}H incorporation.

(G) Comparison of p300 HAT activity toward H3K18 and H3K122 in free and chromatinized H3 in vitro. HAT assay was performed as described above but in the presence of non-radioactive AcCoA. Histone H3 (in octamers or chromatin) was acetylated by p300 in the presence of GAL4-VP16, digested with ArgC and subjected to mass spectrometry. The ratio of unmodified to acetylated peptides was quantified as follows: The XIC values of peptide VTIMPKDIQLAR (positions 118–129) and RKSTGGKAPRK (positions 10–18) with or without acetylation at H3K122 and H3K18 were extracted (four technical replicates). Based on the XIC values, a ratio between unmodified and acetylated peptides for H3K122 and H3K18 was calculated (Kun/Kac). The Kun/Kac ratio was compared between chromatin (set as 1) and free histone octamers both for H3K18 and for H3K122. Based on this H3K18 was 3.2 times more efficiently acetylated in octamers than in chromatin, whereas H3K122 was 214 times more efficiently acetylated.

(H) Knockdown of HATs. MCF-7 cells that were transfected with different siRNAs as indicated were analyzed for knockdown of targeted mRNAs by qRT-PCR 72h after transfection. mRNA was normalized to GAPDH and plotted relative to control siRNA. Concentration of siRNA was: control 50nmol, p300 25nmol, CBP 10nmol, pCAF 25nmol, GCN5 50nmol.

(I) MCF-7 cells were transfected with control or pCAF- and/or GCN5-specific siRNA and were analyzed for different histone modifications 72h after transfection by immunoblotting with antibodies as indicated. Ponceau staining shows equal loading.

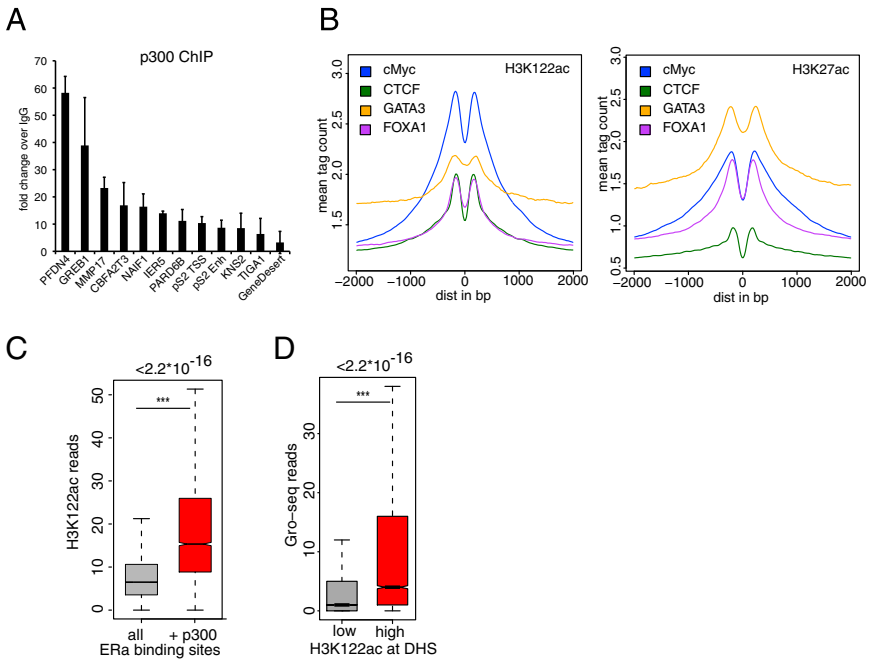

Figure S5. H3K122ac Is a Mark of Active Enhancers, Related to Figure 5

(A) p300 ChIP-Seq validation. Specific enrichment of p300 detected by ChIP-Seq. 'Gene Desert' serves as negative control region. Shown is the average (-/+SD) from two experiments. Primers are listed in Table S3.

(B) H3K122ac and H3K27ac enrichment at genome-wide binding sites of different transcription factors. Aggregation plots show the mean tag count for H3K122ac (left) and H3K27ac (right) at the binding sites of different transcription factors (ENCODE Project Consortium, 2011) as indicated. Note the difference in the relative level of H3K122ac and H3K27ac enrichment around the different transcription factor binding sites.

(C) H3K122ac is enriched at ERα binding sites co-occupied by p300. Box plot shows H3K122ac reads for all ERBSs (gray) or those co-occupied by p300 (red).

(D) DHSs with high levels of H3K122ac (top 10%) are source of significantly more eRNA transcripts compared to the remaining DHSs with lower enrichment of H3K122ac ($p < 2.2*10^{-16}$).

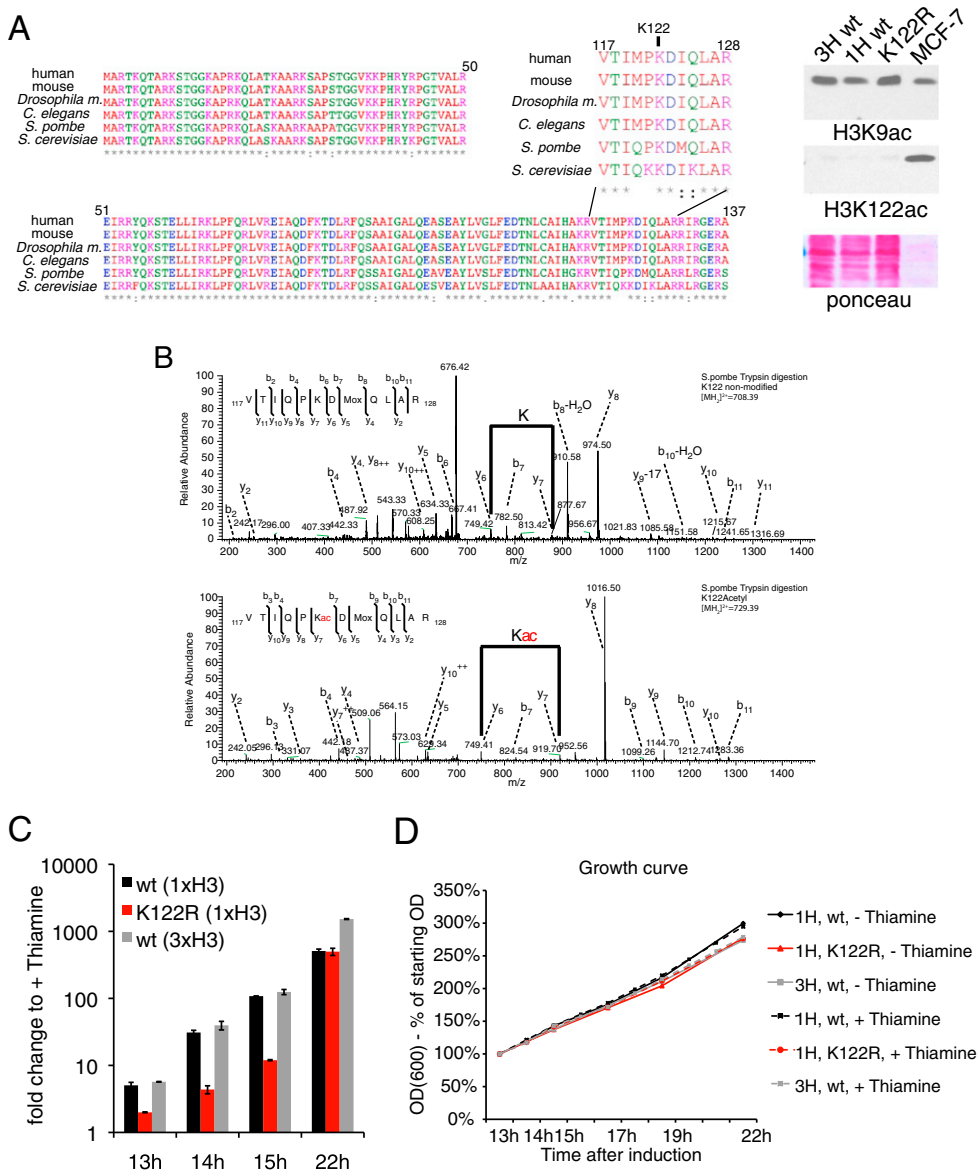

Figure S6. Absence of H3K122ac Impairs Transcriptional Activation In Vivo, Related to Figure 6

(A) ClustalW alignment of the amino acid sequence of human, mouse, *Drosophila*, *C. elegans*, *S. pombe* and *S. cerevisiae* H3.3 (or H3 for *S. cerevisiae*). The enlarged region shows the residues surrounding H3K122 (V117 to R128). Note differences in charge and/or hydrophobicity in residues M120→Q, P121→K and Q125→K between higher eukaryotes and *S. cerevisiae*, whereas *in S. pombe* there are only two charge-neutral substitutions M120→Q (hydrophobicity) and I124→M (neutral). Despite generally high acetylation levels (immunblot on the right, H3K9ac), recognition of H3K122ac by immunoblot is disturbed (right) by changes in the H3K122 epitope and thereby complements controls for antibody specificity in Figure 1.

(B) CID tandem MS spectra of the tryptic *S. pombe* histone H3 peptide VTIMQK$_{122}$DMQLAR in both its unmodified and its acetylated form. The m/z values of the peptides are shown in the upper right corner. The top spectrum shows the unmodified, the bottom spectrum the modified peptide with a mass shift of ~42-Da in the ion series between the y6 and the y7 ion, which indicates the presence of an acetyl group at H3K122 (Kac). The assigned b- and y-type ions are depicted in the spectra, Mox indicates the oxidated state of methionine at position 124. The high mass accuracy of ~2ppm allowed unambiguous discrimination of tri-methyl from H3K122 acetyl modification. Acetylation of K122 was also confirmed by ETD spectra of the same tryptic peptide (data not shown).

(C) Illustrates the same as Figure 6B, but additionally includes data for a *S. pombe* strain with 3 endogenous H3 gene copies. This shows that fission yeast strains containing one instead of three endogenous WT histone H3 gene copies have comparable *nmt1+* gene induction kinetics (see also Mellone et al. [2003]). Shown is the average from three technical replicates (-/+ SD) of a representative experiment.

(D) Growth curve of fission yeast strains analyzed in this study. The OD at 600nm was measured each hour during exponential growth (13–22 hr after induction) and expressed as a percentage of the starting OD.